RTM-Based Downscaling of Medium Resolution Soil Moisture Using Sentinel-1 Data Over Agricultural Fields

Thomas Weiß, Thomas Jagdhuber, *Senior Member, IEEE*, Thomas Ramsauer, Alexander Löw, and Philip Marzahn

***Abstract*—High temporal soil moisture at field scale resolution (10 m–100 m) is important for smart farming decisions. Although, medium and coarse resolution (1 km–50 km) soil moisture information is operationally available on a large scale, high resolution (field scale) datasets are not. This study propose a data assimilation approach to downscale medium resolution (1 km × 1 km) soil moisture information–of intense agriculturally cultivated areas–to field scale. For achieving high transferability of the proposed method, the used input data (Sentinel-1 VV backscatter, Sentinel-2 derived vegetation water content, literature values) can be provided systematically from global operational satellites. Microwave and optical data are used together as input data of a radiative transfer model to derive soil moisture information with high temporal and spatial resolution. The retrieval approach shows a mean ubRMSE for soil moisture estimates of all test fields (Munich-North-Isar test site, Bavaria, Germany) with 0.045 m^3/m^3 and 0.037 m^3/m^3 for 2017 and 2018. Furthermore, the retrieved soil moisture estimates cover a broad range of values from 0.05 m^3/m^3 to 0.4 m^3/m^3. In addition, the temporal evolution of the soil moisture patterns are in line with precipitation events. Moreover, the drying behavior is matched as well. The proposed method showed that for the test area, high resolution soil moisture time series can be provided by only using remote sensing derived input data. In this way, this study is another step towards providing high spatio-temporal soil moisture information for precision farming purposes.**

***Index Terms*—Radiative transfer, Sentinel-1, Sentinel-2, soil moisture, time series, vegetation water content (VWC).**

I. Introduction

SOIL moisture has an indisputable impact on climate, hydrological, and agricultural systems [1], [2], [3]. As soil moisture has a high variability in time and space, continuous monitoring is essential [4], [5]. Moreover, different model applications, flood forecasting, or precision farming rely heavily on spatio-temporal distributed soil moisture information. Compared to remote sensing derived soil moisture products, traditional in-situ measurements at the point scale are expensive and fall short of providing spatio-temporal patterns on a larger (e.g., subcatchment) scale [6]. Today, several operational NASA and ESA missions (Soil Moisture Active Passive (SMAP), Soil Moisture and Ocean Salinity (SMOS), or Advanced SCATterometer (ASCAT)) produce global soil moisture maps at a coarse spatial resolution of 25 km to 50 km [7]. Further products of medium spatial resolution (1 km to 10 km) are mostly achieved by downscaling coarse resolution products [8], [9] or combining information from coarse and medium/high resolution sensors [10], [11]. Thus, medium resolution soil moisture products are available at a regional scale, e.g., a RADOLAN (radar online calibration)-based soil moisture product for Germany (RADOLAN Antecedent Precipitation Index—A Soil Moisture Dataset derived from Weather Radar Data; Ramsauer et al. [12]) or a SMAP-based product for China [13]. Other soil moisture products provided by the Copernicus Global Land Service [10] or NASA [11] reach even global coverage. However, global and regional products differ in their retrieval approach as well as in temporal (hourly to several days) and spatial resolutions. Compared to the the 1 km RADOLAN product which offers absolute soil moisture values in vol.%, the 1 km Copernicus soil moisture product is a change detection approach which leads to relative soil moisture values in % from 0 to 100. However, compared to medium resolution soil moisture products, operationally produced high resolution (field scale, meaning below 1 km) datasets on a global scale are not yet available [7]. But regional studies using polarimetric decomposition [14], [15], machine learning approaches [16], data fusion [17], statistical modeling [18], or radiative transfer models (RTMs) [19] show promising results in estimating soil moisture from synthetic aperture radar (SAR) data at the field scale. The use of RTMs and radar observations has been proven to be a suitable approach [20], [21]. With RTM a logical linkage between observations and physical processes can be established [22]. Thus, a better physical understanding as well as simulations of interactions between electromagnetic waves and the land surface is possible. Furthermore, RTMs are not only able to interpret satellite measurements, but also capable

Received 29 April 2024; revised 25 June 2024 and 8 August 2024; accepted 15 August 2024. Date of publication 23 August 2024; date of current version 9 September 2024. *(Corresponding author: Thomas Weiß.)*

Thomas Weiß is with the Department of Geography, Ludwig-Maximilians-Universität of Munich, 80333 Munich, Germany, also with the Faculty of Agricultural and Environmental Sciences, University of Rostock, 18059 Rostock, Germany, and also with the Fraunhofer Insitut for Computer Graphics Research (IGD), University of Rostock, 18059 Rostock, Germany (e-mail: weiss.thomas@lmu.de).

Thomas Jagdhuber is with the German Aerospace Center, Microwaves and Radar Institute, 82234 Weßling, Germany, and also with the Faculty of Applied Computer Science, Institute of Geography, University of Augsburg, 86159 Augsburg, Germany.

Thomas Ramsauer and Alexander Löw are with the Department of Geography, Ludwig-Maximilians-Universität of Munich, 80333 Munich, Germany.

Philip Marzahn is with the Faculty of Agricultural and Environmental Sciences, University of Rostock, 18059 Rostock, Germany.

Digital Object Identifier 10.1109/JSTARS.2024.3448625

of providing predictions under different conditions [23]. For bare soil applications, forward models of Oh [24], [25], Dubois [26], or the Integral Equation Model developed by Fung et al. [27] are often applied, among others. A study by Baghdadi et al. [28] showed that the accuracy on plot scale of bare soil moisture estimates is highly dependent on the surface roughness state. By using Sentinel-1 images an overestimation of soil moisture by high soil roughness and an underestimation of soil moisture by low surface roughness is observed [28]. For vegetated areas, the bare soil models need to be combined with vegetation scattering models. Here, the Water Cloud Model (WCM) approach by Attema and Ulaby [29] or a Single Scattering Radiative Transfer (SSRT) [30], [31] model is used for inverting radar backscatter to retrieve soil moisture information. The main uncertainty of radar based soil moisture retrievals in vegetated areas is the influence of the canopy layer on the backscatter signal [32], [33], [34]. The WCM considers the canopy layer as a collection of identical spherical particles, that are uniformly distributed [29]. Thus, the vegetation contribution within WCM (only considering direct scattering contributions from plants) is simplified by not differentiating between additional occurring scattering mechanisms (plant–ground, ground–plant, or ground–plant–ground scattering contributions). In contrast, the SSRT distinguishes the canopy layer by scattering mechanisms, so direct vegetation contribution as well as canopy–soil and soil–canopy–soil interactions are considered [31]. For accurate soil moisture retrievals, information about vegetation in terms of crop type, structure, phenology, and water content is necessary. Therefore, Vegetation Optical Depths (VOD), Normalized Difference Vegetation Index (NDVI), Normalized Difference Water Index (NDWI), or Vegetation Water Content (VWC) are used as remote sensing-based indicators from optical and radar observations. [35], [36], [37]. Over large areas, optical remote sensing data has proven useful in obtaining information on vegetation at field resolution. [38], [39], [40]. Thus, a combination of SAR (Sentinel-1) and optical data (Sentinel-2) provides unique possibilities for improving soil moisture estimates by using microwave RTMs with additional information provided by optical sensors [41], [42].

This article aims to investigate the potential of accurate downscaling of a soil moisture product at medium resolution (1 km) to field scale by combining high-resolution SAR and optical remote sensing data based on RTM. The approach is deliberately based on a few input parameters, which can already be derived from remote sensing sensors, to ensure easy transferability of the approach to other areas worldwide. The used remote sensing information are a RADOLAN-based soil moisture product at 1-km resolution, VV-polarized backscatter (Sentinel-1), and as a vegetation descriptor, the VWC (calculated from NDWI information obtained from Sentinel-2). The spatio-temporal distributed data is used to drive an inversion process for models Oh04 and SSRT. Thus, a time series of almost daily spatially distributed absolute soil moisture estimates (Vol.%) is achieved.

II. Datasets

A. Test Site

For our study, the Munich-North-Isar (MNI) test site [43], [44] with in-situ measurements of winter wheat and maize fields for the years 2017 and 2018 was chosen. The winter wheat fields were sowed beginning of October and harvested mid/end of July in both years. The maize fields were sowed end of May in 2017 and beginning of May in 2018. The harvest of the maize took place end of September in 2017 and beginning of September in 2018. Besides the two main crop types (wheat and maize), grassland is the third major type of agricultural cultivation. The test site (48°13′N–48°20′N, 11°39′E–11° 45′E, Fig. 1) is located near Munich, southern Germany. Two meteorological stations (Eichenried and Grub) provide measurements within a 15-km radius around the study area. For the year 2017, the measurements show an annual mean temperature of 9.3 °C (Eichenried) and 9.5 °C (Grub). Furthermore, an average annual precipitation of 853 mm (Eichenried) and 863 mm (Grub) was observed in 2017. For the year 2018, the measurements show a higher annual mean temperature of 10.3 °C (Eichenried and Grub) and a more diverse average annual precipitation of 663 mm (Eichenried) and 926 mm (Grub). The river Isar within the test site is embanked and has no significant influence on the water availability of the agricultural areas in the vicinity. Furthermore, no irrigation practices were observed during the years 2017 and 2018 within the MNI test site.

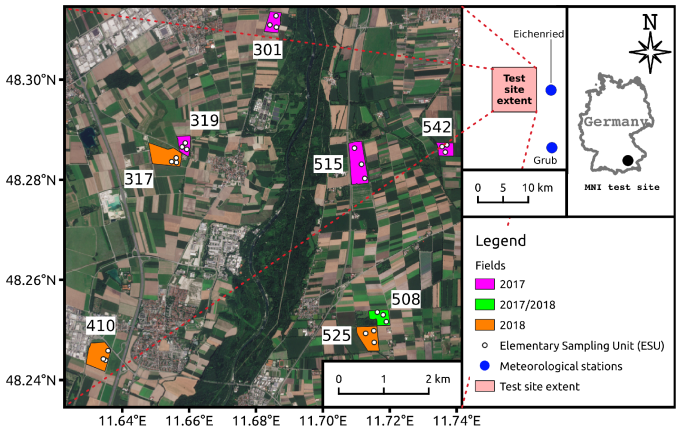

Fig. 1. Munich-North-Isar (MNI) test site with sampled wheat and maize fields of 2017 and 2018. The inset map shows the spatial relationship between meteorological stations and the test site.

B. In-Situ Data

For 2017, in-situ data comprising five different fields (three wheat and two maize fields) and for 2018, measurements of four different fields (two wheat and two maize fields) are available for detailed and local analyses. Field measurements were taken at three different locations (Elementary Sampling Points ESU) on every test field. At each location, the plants of half a square meter were taken, the wet and dry (drying temperature 102°C) weights of the plants were measured, and the VWC was calculated. Soil moisture time series were provided by permanently installed sensors (Decagon TM5 sensors, Decagon Devices Inc., Pullman, WA, USA) within the upper soil layer (first five centimeters). The monitoring interval was ten minutes. Further information about the in-situ measurements are summarized in Table I.

TABLE I
ACQUISITION TIME, TIME INTERVAL, AND RANGE OF IN-SITU MEASUREMENTS (VEGETATION WATER CONTENT AND SOIL MOISTURE)

Variable	Type	Acquisition time 2017	Acquisition time 2018	Range	Time interval
VWC [kg/m^2]	Wheat	03/24 – 07/17	04/04 – 07/13	0.04 – 6.3	weekly
	Maize	06/08 – 09/22	05/25 – 08/29	0.02 – 10.2	
Soil Moisture [m^3/m^3]	Wheat	03/24 – 07/17	04/20 – 07/13	0.02 – 0.38	ten minutes
	Maize	07/06 – 09/22	05/16 – 08/29	0.03 – 0.39	

TABLE II
USED REMOTE SENSING DATA FOR MNI TEST SITE OF 2017 (03/24/2017-09/22/2017) AND 2018 (04/04/2018-08/29/2018)

Data set	Amount 2017	Amount 2018	Bands	Resolution [m]
Sentinel-1	121	86	VV	10×10
Sentinel-2	16	17	8a, 11	20×20
RADOLAN API	–	–	–	1000×1000

C. Remote Sensing Data

1) Sentinel-1: The Sentinel-1 satellites (C-band) provide continuous images for the MNI test site. In 2017 and 2018, Sentinel-1A and Sentinel-1B provide four different overpasses (relative orbit number 44,95,117,168) The MNI test site is observed with two incidence angle sets of 35°–36° and 43°–45°. The usage of all available scenes led to an average temporal revisit time of 1.5 days. The Level-1 Single Look Complex (SLC) data product was preprocessed by using the default configuration for time series processing of the python package SenSARP [45]. SenSARP utilizes ESA's SNAP Toolbox to apply thermal noise removal, radiometric calibration, geometric correction, radiometric correction, co-registering, and multitemporal speckle filtering. Thus, a radiometric and geometric corrected as well as temporal speckle filtered time series of Sentinel-1 images is provided. El Hajj et al. [46] and Baghdadi et al. [47] suggested that VV polarization is more suitable to monitor soil moisture under well-developed agricultural vegetation than VH. Therefore, VV polarized backscatter is the main focus of the study. Table II summarizes the information from the used Sentinel-1 images.

2) Sentinel-2: Sentinel-2 satellites provide free multispectral data with systematic global coverage. The Multispectral Imager sensor on Sentinel-2 has 13 spectral bands covering wavelength from 443 nm (Ultra Blue) to 2190 nm (Short Wave Infrared (SWIR). The spatial resolution of different bands ranges from 10to 60 m. Within our study a combination of Bands B8a (10 m, 842 nm—Visible and Near Infrared) and B11 (20 m, 1610 nm—SWIR) is used. Observations from Sentinel-2 of the MNI test site are available every 2–3 days. However, only 32 images for the time period under investigation (2017 + 2018) have a cloud coverage below 10% and were therefore used in this study. The Sentinel-2 images are preprocessed and retrieved using the Google Earth Engine. In order to transform the top-of-atmosphere to surface reflectance values and hence account for atmospheric artifacts in the imagery, the 6S radiative transfer code is used [48], [49]. Table II summarizes the information from the Sentinel-2 data.

3) RADOLAN API: The utilized RADOLAN API dataset [50] is an empirically retrieved soil moisture dataset based on the German weather radar product RADOLAN RW [51], [52]. It extends the idea of the Antecedent Precipitation Index (API) [53], integrating information on local soil characteristics (SoilGrids; Hengl et al. [54]) and spatially distributed temperature data. The algorithm accounts for general physical boundaries in soil hydrology (e.g., moisture content limits) when empirically modeling saturation state dependent soil moisture gains and losses. The hourly RADOLAN API dataset with a spatial resolution of 1 km × 1 km is openly available for the spatial domain of Germany (utilized version 1.0.0 (2015–2019)) [12].

D. CORINE Land Cover

The CORINE land cover class 2 from 2018 [55], in particular 211 ("nonirrigated arable land") and 231 ("pasture, meadows, and other permanent grasslands under agricultural use") are used as a mask. Thus the algorithm is only applied on agricultural areas excluding vineyards and forest areas. It has to be mentioned that although forestry areas are excluded some scrub vegetation/forestry areas are wrongly found within the 211 and 231 CORINE land cover classes.

III. METHODOLOGY

The main objective is the development of an approach to downscale a medium resolution soil moisture product to field scale by using RTMs. The proposed method was developed and tested at a test site in southern Germany, Bavaria. Enabling transferability to other regions, the focus during method development was set on a minimal set of input parameters for the RTMs, which can already be operationally derived by remote sensing products.

A. Radiative Transfer Model

This section introduces a first order radiative transfer model (SSRT), which is used in an inversion process for the retrieval of soil moisture information in agricultural areas with vegetation cover. The original SSRT [30], [31] can be described as

$$\sigma^0_{pq} = \sigma^0_{g_{pq}} + \sigma^0_{c_{pq}} + \sigma^0_{cgt_{pq}} + \sigma^0_{gcg_{pq}}. \quad (1)$$

An overview of the different scattering contributions simulated by SSRT is given in Fig. 2. The ground contribution $\sigma^0_{g_{pq}}$ (p and q stand for the polarization) can be further described by

$$\sigma^0_{g_{pq}} = T_p T_q \, \sigma^0_{s_{pq}} \quad (2)$$

where $\sigma^0_{s_{pq}}$ represents the surface scattering and T_p and T_q are the transmissivity of the canopy for the respective polarization. The transmissivity (11) accounts for the signal loss of the surface scattering when passing through the canopy covers. For the surface scattering, the model of Oh [25] (Oh04) is used. Oh04

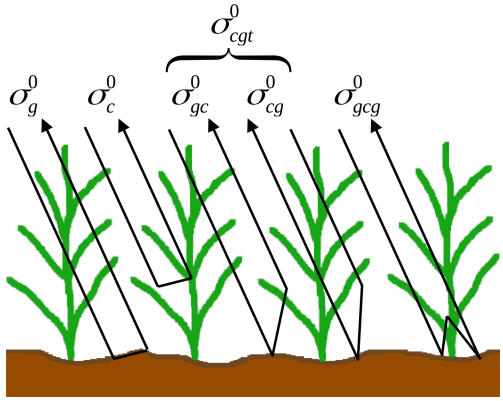

Fig. 2. SSRT modeled scattering contributions in a vegetation canopy. Direct backscatter from soil (σ^0_g), direct backscatter from plants (σ^0_c), ground–plant (σ^0_{gc}), plant–ground (σ^0_{cg}) scattering, and ground–plant–ground scattering σ^0_{gcg}). Figure adapted from Ulaby and Long [31].

is a semiempirical model that was developed by using in-situ measurements of a variety of soil types, primarily silt loam, loam, and sandy loam [56]. One advantage of Oh04 is that no additional information about the soil type is necessary. The authors claim that the backscatter has only a weak dependency on soil type but is, in comparison, highly influenced by soil moisture (sm) and surface roughness [56]. The backscatter $\sigma_{s_{VV}}$ of Oh04 is defined as

$$\sigma^0_{s_{VV}} = \frac{0.11\ sm^{0.7}\ (\cos\theta)^{2.2}\ \left[1 - e^{-0.32\ (ks)^{1.8}}\right]}{0.095\ (0.13 + \sin^{1.5}\theta)^{1.4}\ \left[1 - e^{-1.3\ (ks)^{0.9}}\right]}. \quad (3)$$

Therefore, the soil moisture by Oh04 can be calculated with information about the backscatter $\sigma^0_{s_{VV}}$, the local incidence angle θ, and the soil roughness ks. The soil roughness can be further specified by k as the radar wave number ($k = 2\pi/\lambda$) and s as the rms height of the soil surface. The rms height (s) characterizes the surface height variation and as such describes the scattering effects of natural surfaces in the vertical domain (profile). Furthermore, the soil roughness is dependent on the sensor wavelength (λ). The canopy scattering components of the SSRT [30], [31] are defined as

$$\sigma^0_{c_{pq}} = \frac{\sigma^{\text{back}}_{V_{pq}}\ \cos\theta}{k^p_e + k^q_e}\ (1 - T_p T_q), \quad (4)$$

$$\sigma^0_{cgt_{pq}} = \sigma^{\text{bist}}_{V_{pq}}\ H\ [R_p + R_q]\ T_p T_q \quad \text{and} \quad (5)$$

$$\sigma^0_{gcg_{pq}} = \frac{\sigma^{\text{back}}_{V_{pq}}\ \cos\theta}{k^p_e + k^q_e}\ (R_p R_q - T_p T_q) \quad (6)$$

with θ as incidence angle, H as canopy height, and R represents the Fresnel coefficients of the respective polarization. The Fresnel coefficients for horizontal R_H and vertical R_V polarization are defined [31] as

$$R_H = \frac{\mu_r \cos\theta - \sqrt{\mu_r \epsilon_r - \sin^2\theta}}{\mu_r \cos\theta + \sqrt{\mu_r \epsilon_r - \sin^2\theta}}, \quad (7)$$

$$R_V = \frac{\epsilon_r \cos\theta - \sqrt{\mu_r \epsilon_r - \sin^2\theta}}{\epsilon_r \cos\theta + \sqrt{\mu_r \epsilon_r - \sin^2\theta}} \quad (8)$$

where μ_r is the relative permittivity. Under the assumption of isotropic canopy scatterers [31] following relationship is assumed for the volume backscattering coefficient $\sigma^{\text{back}}_{V_{pq}}$ and the volume bistatic scattering coefficient $\sigma^{\text{bist}}_{V_{pq}}$:

$$\sigma^{\text{bist}}_V = \sigma^{\text{back}}_V = k_s. \quad (9)$$

The scattering component k_s is defined by the single scattering albedo ω and the extinction coefficient k_e as

$$k_s = \omega\ k_e. \quad (10)$$

The transmissivity T for the polarization p can be written as

$$T_p = e^{-k^p_e\ H\ \sec\theta} \quad (11)$$

whereas $k^p_e\ H$ is often referred to as VOD. VOD can be retrieved from passive and active microwave systems. In the passive domain empirical studies showed a good correlation between VOD and the Vegetation Water Content (VWC). Thus, VOD can be expressed by $k^p_e\ H$ (active microwave domain) and b VWC (passive microwave domain) as

$$\text{VOD} = k^p_e\ H = b\ \text{VWC} \quad (12)$$

where the b parameter from the passive domain is empirical derived and depends on vegetation type, structure, growth stage, and water status [57], [58]. The Soil Moisture Active Passive (SMAP) mission uses a static b parameter differentiated by land cover type. However, recent studies found that b does vary throughout the vegetation season due to significant change of crop water [58], [59]. Thus, in order to archive a temporal dynamic for b along the growing period, we found that linking b to a normalized VWC parameter (range 0 to 1) works quite well for the active microwave domain. Therefore, the utilized b in our case can be written as

$$b = b'\ \text{VWC}^{\text{norm}} \quad (13)$$

with VWC^{norm} for a specific timestep i as

$$\text{VWC}^{\text{norm}}_i = 1 - \frac{\text{VWC}_i - \min(\text{VWC})}{\max(\text{VWC}) - \min(\text{VWC})}. \quad (14)$$

The min and max values of the VWC are calculated on pixel basis and for each growing period separately. Due to the inversion within (14), VWC^{norm} decreases while the original VWC increases. Based on the VWC normalization in (14) the dependency of b and also of VOD changes to a more parabolic form which helps the algorithm fitting process. In order to better distinguish between the original tranmissivity of the SSRT model (T) and the introduced changes, we refer the used transmissivity as T'. Combining (11), (12), and (13), the used transmissivity of the canopy T' can be written as

$$T'_p = e^{-b\ \text{VWC}\ \sec\theta} \quad (15)$$

$$T'_p = e^{-b'\ \text{VWC}^{\text{norm}}\ \text{VWC}\ \sec\theta}. \quad (16)$$

To minimize the required input parameters, a literature value for the single scattering albedo ($\omega = 0.03$) [20], [60] was used.

Furthermore, during the analysis published in Weiß et al. [20] and Weißet al. [60] the vegetation height H was found to be a nonsensitive parameter within (5) and thus in absence of height information, H=1 m is assumed. Thus, considering only polarization VV the final equations for the canopy scattering component can be written as

$$\sigma^0_{c_{VV}} = \frac{1}{2}\,\omega\,\cos\theta\,(1 - T'_V T'_V), \tag{17}$$

$$\sigma^0_{cgt_{VV}} = \omega\,b'\,\mathrm{VWC}^{\mathrm{norm}}\,\mathrm{VWC}\,[R_V + R_V]\,T'_V T'_V, \tag{18}$$

$$\sigma^0_{gcg_{pq}} = \frac{1}{2}\,\omega\,\cos\theta\,(R_V R_V - T'_V T'_V) \tag{19}$$

by considering R_V (8) and T'_V (16).

B. Vegetation Water Content (VWC)

VWC is often used as a parameter to characterize the vegetation above the ground. But unlike, e.g., NDWI, VWC cannot be easily measured by optical satellites such as Sentinel-2. Nevertheless, a high correlation between VWC and NDWI was found in numerous studies (R^2: 0.57–0.89) [39], [61], [62], [63]. The NDWI_{1640} is described as

$$\mathrm{NDWI}_{1640} = \frac{\mathrm{NIR}_{860} - \mathrm{SWIR}_{1640}}{\mathrm{NIR}_{860} + \mathrm{SWIR}_{1640}} \tag{20}$$

where the near infrared channel at λ=860 nm (NIR_{860}) and short wave infrared channel at λ=1640 nm (SWIR_{1640}) corresponded to Band 8a and Band 11 of the Sentinel-2 satellites. For a NDWI-based VWC calculation, several crop type specific empirical equations exist in the literature [39]. For simplicity of the approach, we used the wheat specific equation in Maggioni et al. [62] to calculate the VWC for the entire test site. The equation for VWC over wheat fields from Maggioni et al. [62] is

$$\mathrm{VWC} = 13.2\,\mathrm{NDWI}^2_{1640} + 1.62\,\mathrm{NDWI}_{1640}. \tag{21}$$

C. Soil Moisture Downscaling Approach

The RTM combination Oh04 and SSRT (Section III-A) is used in an inversion process to downscale a medium resolution soil moisture dataset (RADOLAN API [50]) by using a cost function J, defined as

$$J = J_{\mathrm{obs}} + J_{\mathrm{prior}} \tag{22}$$

and minimized by **L**imited-memory **B**royden-**F**letcher-**G**oldfarb-**S**hanno with **B**ox constraint (L-BFGS-B) [64] which is a gradient descent approach. The cost function is described by the model fit to the observations J_{obs} and deviations from a priori information J_{prior} of the observation variables. J_{obs} as the mismatch between Sentinel-1 backscatter and modeled RTM backscatter is described by

$$J_{\mathrm{obs}} = \frac{1}{2}(y - H(x))^T C_0^{-1}(y - H(x)) \tag{23}$$

where y is the time series of Sentinel-1 VV polarized radar backscatter (σ^0_{VV}). $H(x)$ is the RTM backscatter with x describing the state variables sm (3), VWC (21), b (13), and rms height s (3). The observation uncertainty is represented by the covariance

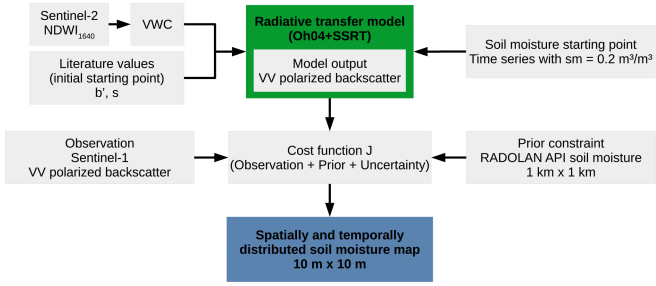

Fig. 3. Schematic illustration of methodology.

matrix C_0. Another important part of the optimization process is the prior information. Thus, J_{prior} is defined as

$$J_{\mathrm{prior}} = \frac{1}{2}(x - x_p)^T C_P^{-1}(x - x_p) \tag{24}$$

with a vector x again describing the state variables, x_p referring to the prior estimates, and the covariance matrix C_P as the uncertainty of the prior. Before the start of the parameter estimation process, realistic boundaries based on the model physics as well as a starting value were set for the applied optimization algorithm L-BFGS-B. The possible equifinality problem in an underdetermined system is addressed by the usage of a guided optimization (weak constraint) approach. The derived parameters (sm, VWC, b', and s) are not completely unknown parameters. Due to the absence of tillage practices rms height s is assumed to be static throughout the vegetation growing period, thus only one value for s for each pixel needs to be optimized. Prior information for sm (RADOLAN API) and VWC (derived from Sentinel-2 observations) as well as literature values for the initial starting points of b' and s form in conjunction with provided uncertainty information a weak constraint data assimilation system [65], [66]. An overview of the boundaries, priors, starting values, and uncertainty ranges is given in Table III. During the inversion process, the entire state vector (sm, VWC, b', and s) is optimized for each satellite pixel by comparing the entire time series of Sentinel-1 VV polarized backscatter with a time series of RTM derived backscatter values that depend on the respective state vector values, priors (sm, VWC), boundaries (sm, VWC, b', s) and uncertainty (VV backscatter, sm, VWC, b', s). The optimized state vector values for sm, VWC, and b' are allowed to differ between each time step, whereas for rms height s only one value for the entire time series is optimized. The entire methodology is schematically illustrated in Fig. 3.

D. Applied Statistical Metrics

For the evaluation of the RTM based soil moisture downscaling approach, statistical metrics were used. The Root Mean Square Error (RMSE), the bias, the unbiased Root Mean Square Error (ubRMSE), the correlation coefficient R and the coefficient of variation (CV) are defined as

$$\mathrm{RMSE} = \sqrt{\frac{1}{N}\sum_{i=1}^{N}(P_i - O_i)^2} \tag{25}$$

TABLE III
APPLIED PARAMETER BOUNDARIES, PRIORS, STARTING VALUES, AND UNCERTAINTY RANGES

Parameter	Boundaries	Prior	Starting point	Uncertainty
sm [m^3/m^3]	0.01 – 0.7	API	0.2	0.13
VWC [kg/m^2]	0 – 7.5	Sentinel-2	Sentinel-2	0.1
s [m]	0.005 – 0.03	–	0.025	0.1
b [Npm^2/kg]	0 – 1	13	0.4/0.6	0.5
VV backscatter [dB]	–	–	–	1

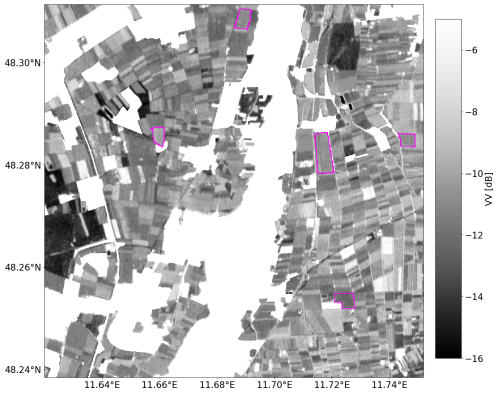

Fig. 4. Mean Sentinel-1 VV backscatter (10 m × 10 m) of investigation time period March to September 2017.

Fig. 5. Sentinel-2 derived mean VWC (20 m × 20 m) of investigation time period March to September 2017.

$$\text{bias} = \frac{1}{N}\sum_{i=1}^{N}(P_i - O_i) \tag{26}$$

$$\text{ubRMSE} = \sqrt{\frac{1}{N}\sum\nolimits_{i=1}^{N}[(P_i - bias) - O_i]^2} \tag{27}$$

$$\text{R} = \frac{\sum_{i=1}^{N}[(P_i - \overline{P})(O_i - \overline{O})]}{\sqrt{\sum_{i=1}^{N}(P_i - \overline{P})^2 \sum_{i=1}^{N}(O_i - \overline{O})^2}} \tag{28}$$

$$\text{CV} = \frac{\sigma}{\mu} \tag{29}$$

with N as total number of observation, O_i as ith observation, P_i as ith prediction, $\overline{O}$ and $\overline{P}$ as average of observation and predictions, σ as standard deviation, and μ as mean.

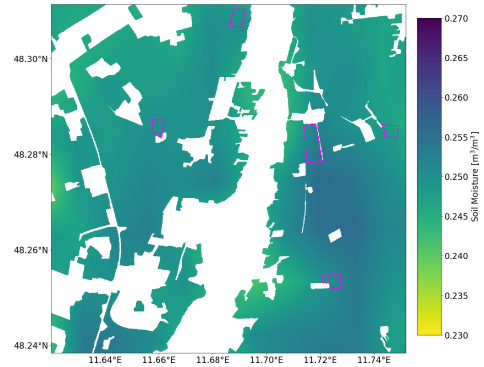

Fig. 6. Mean value of RADOLAN API soil moisture (1 km × 1 km) of investigation time period March to September 2017.

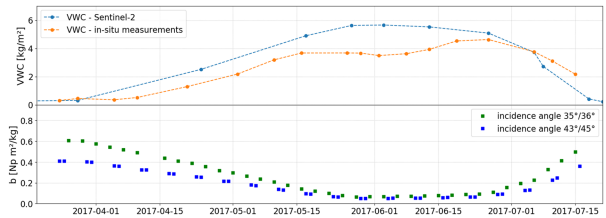

Fig. 7. VWC and evolution of b for winter wheat field 508.

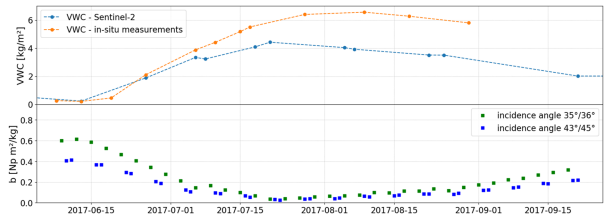

Fig. 8. VWC and evolution of b for maize field 515.

IV. RESULTS

A. Spatial Distributed Model Input

Spatially distributed model input data are the VV-polarized Sentinel-1 backscatter (Fig. 4), Sentinel-2 derived VWC (Fig. 5), and a coarse resolution soil moisture product based on RADOLAN data (Fig. 6). Looking at the high resolution (10 m × 10 m) mean VV backscatter (Fig. 4) for the investigation time period of March to September 2017, field boundaries are clearly visible, whereas intra-field differences are low. The mean backscatter of the entire scene is 10.5 dB for 2017 and 10.7 dB for 2018. Certain areas with low backscatter values (black/dark color) correspond to forestry or other nonagricultural areas, which will not be considered in the quality assessment of the

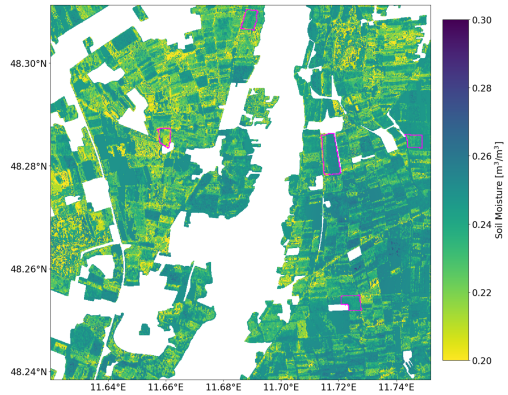

Fig. 9. Mean downscaled high resolution soil moisture (10 m × 10 m) of investigation time period March to September 2017.

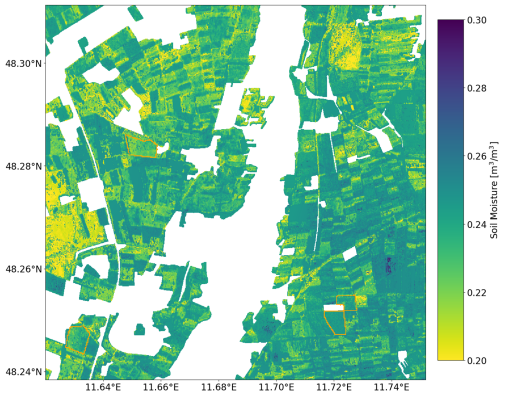

Fig. 12. Mean downscaled high resolution soil moisture (10 m × 10 m) of investigation time period April to September 2018.

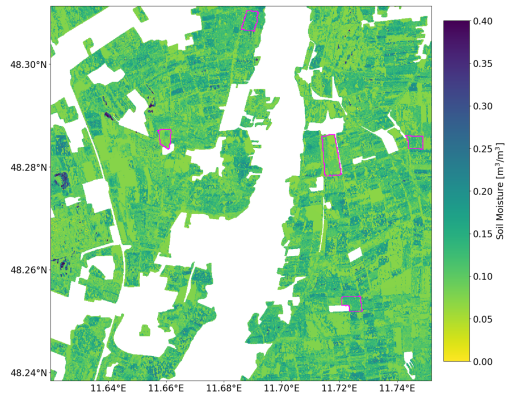

Fig. 10. Coefficient of variation of downscaled high resolution soil moisture of investigation time period March to September 2017.

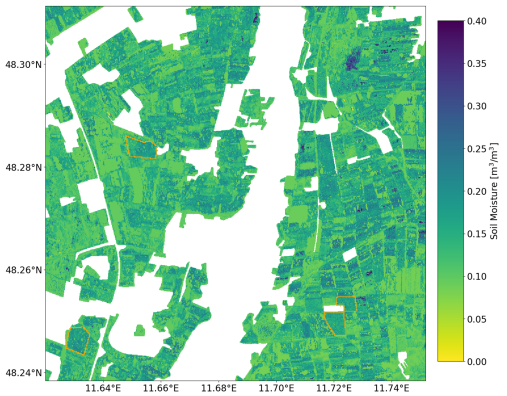

Fig. 13. Coefficient of variation of downscaled high resolution soil moisture of investigation time period April to September 2018.

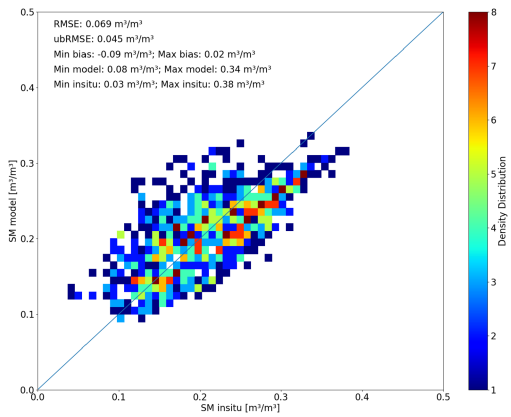

Fig. 11. Unbiased in-situ soil moisture (five fields with three ESUs) compared with downscaled soil moisture of year 2017.

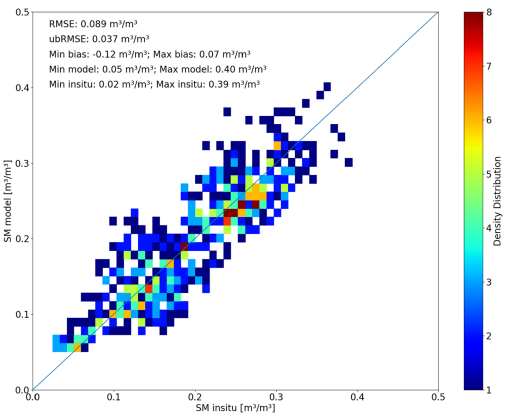

Fig. 14. Unbiased in-situ soil moisture (four fields with three ESUs) compared with downscaled soil moisture of year 2018.

approach later on. Field boundaries can be distinguished within the high resolution (20 m × 20 m) mean VWC image (Fig. 4) for the investigation time period of 2017 too. The mean VWC of the entire scene is 1.37 kg/m^2 for 2017 and 1.25 kg/m^2 for 2018. Contrary to the backscatter information, intrafield differences for certain fields (515 or 301) are visible. The coarse resolution (1 km × 1 km) mean RADOLAN API soil moisture product (Fig. 6) for the investigation time period of 2017 shows, compared to the backscatter and VWC, no field boundaries and low overall differences (the legend of soil moisture range is within 0.05 m^3/m^3). The mean soil moisture of the entire scene is 0.25 m^3/m^3 for both years. Input data for the year 2018 is not shown due to similar patterns with small differences in backscatter and VWC content based on field crop rotation.

TABLE IV
PERFORMANCE METRICS (RMSE, BIAS, UBRMSE) FOR DIFFERENT GROWING PERIODS (TS=ENTIRE TIME SERIES; BBCH<40=TILLERING AND STEM ELONGATION; BBCH>39=HEADING, FLOWERING, FRUIT DEVELOPMENT AND RIPENING) AS WELL AS FOR INDIVIDUAL FIELDS SEPARATED BY YEAR AND CROP TYPE

Year	Field	Crop Type	RMSE [m³/m³]			Bias [m³/m³]			ubRMSE [m³/m³]		
			TS	BBCH<40	BBCH>39	TS	BBCH<40	BBCH>39	TS	BBCH<40	BBCH>39
2017	301	Wheat	0.093	0.079	0.100	–0.09	–0.07	–0.08	0.049	0.038	0.048
2017	319	Maize	0.073	0.089	0.043	–0.08	–0.08	–0.03	0.038	0.022	0.025
2017	508	Wheat	0.059	0.018	0.040	–0.01	–0.01	–0.02	0.033	0.018	0.032
2017	515	Maize	0.055	0.058	0.033	–0.03	–0.05	0.01	0.046	0.028	0.032
2017	542	Wheat	0.056	0.039	0.063	0.02	0.03	–0.04	0.053	0.014	0.045
2018	317	Wheat	0.126	0.133	0.117	–0.12	–0.13	–0.11	0.046	0.004	0.043
2018	410	Maize	0.113	0.109	0.105	–0.11	–0.10	–0.10	0.033	0.030	0.028
2018	508	Maize	0.035	0.042	0.027	0.01	0.01	0.02	0.034	0.039	0.015
2018	525	Wheat	0.056	0.021	0.033	0.07	0.02	0.01	0.032	0.008	0.032

B. Parameter b

Figs. 7 and 8 show the change of parameter b based on the temporal evolution of VWC. As the VWC is normalized and multiplied with b ((13)), higher VWC values result in lower b values and vice versa. Figs. 7 and 8 show the Sentinel-2 derived VWC content for wheat field 508 and maize field 515. The derived VWC content matches the temporal evolution of the in-situ measurements quite well ($R > 0.9$). But a slight intensity mismatch between the observed and calculated VWC can be observed for wheat as well as for maize fields. The starting point of b depends on the incidence angle of the respective VV backscatter observations [60].

C. Downscaled Soil Moisture Results

Figs. 9 and 12 illustrate the mean downscaled soil moisture of the investigation time period for 2017 and 2018, respectively. Test fields with in-situ measurements show similar mean soil moisture values despite crop rotation practices between the years. The average soil moisture of the test area for 2017 and 2018 was 0.236 m^3/m^3 and 0.235 m^3/m^3, respectively. Within the test area, different fields show partly differing soil moisture values. Thus, field boundaries are detectable, although not as visible as the boundaries in the input variables of VV backscatter and VWC. In order to analyze the temporal dynamics of soil moisture, Figs. 10 and 13 illustrate the CV of the downscaled soil moisture within the investigation time period for 2017 and 2018. Overall, slightly higher CV values were retrieved for 2018 (mean CV = 0.138) than for 2017 (mean CV = 0.109). This is in line with in-situ observations, which indicate a drier summer and wetter spring for 2018 than for 2017. Isolated pixels within some crop fields show high CV values of > 0.4. These high CV values might be the result of remaining speckle disturbances within the backscatter data. Furthermore, areas with high CV values (> 0.4) show very low mean backscatter values of < -15 dB. A comparison of in-situ and bias corrected downscaled soil moisture for wheat and maize fields are illustrated in Figs. 11 and 14. The mean RMSE for all ESUs is 0.069 m^3/m^3 and 0.089 m^3/m^3 for 2017 and 2018, respectively. Considering the ubRMSE, values of 0.045 m^3/m^3 and 0.037 m^3/m^3 are shown. A higher improvement of RMSE and ubRMSE is seen for 2018, though a higher bias range is calculated for 2018 (Fig. 14) than for 2017 (Fig. 11). Furthermore, both years show a similar range of in-situ soil moisture measurements (2017: 0.03–0.38 m^3/m^3; 2018: 0.02–0.39 m^3/m^3). In addition, a higher soil moisture range is seen within the downscaled values for 2018 (0.05 - 0.40 m^3/m^3) than 2017 (0.08 - 0.34 m^3/m^3). In general, the soil moisture results are well located around the 1:1 line. The performance metrics for the individual fields, separated by year and crop type, are illustrated in Table IV. To differentiate between phenological stages, the **B**iologische **B**undesanstalt, Bundessortenamt and **CH**emical (BBCH) [67] developed a system for uniform coding of growth stages for all mono- and dicotyledonous plant types. Performance metrics for different vegetation growing period can be also found in Table IV as well. Considering the results for the entire time series of the individual fields, no obvious pattern which would suggest that the method works better for wheat or maize fields can be detected. But a high RMSE goes along with a high bias. The ubRMSE for the entire time series shows for all test fields a similar performance of 0.032 to 0.053 m^3/m^3. This indicates that the temporal evolution is well met even for fields with high RMSE values. Comparing the RMSE and ubRMSE of wheat fields, a better RMSE and ubRMSE are observed for BBCH<40 than BBCH>39. This suggests that the retrieval works better for lower vegetation stages. The same behavior can be observed for maize fields in 2017 whereas the results from 2018 are contradicting.

The correlation coefficient and standard deviation of downscaled and in-situ soil moisture values as well as RADOLAN API and in-situ values are illustrated on a field basis in Figs. 15–17. For the results in Fig. 15, the entire investigation period is considered, whereas in Figs. 16 and 17, the time series is separated according to different phenological phases. Fig. 16 shows the soil moisture results for the time period with BBCH values lower than 40 (tillering and stem elongation), and Fig. 17 shows the results with BBCH values higher than 39 (heading, flowering, fruit development, and ripening). Overall, the time series and subsets show a low standard deviation of <0.04 m^3/m^3. The correlation coefficient for the entire time series has a broad range from 0.06 to 0.78 for the RT retrieved soil moisture. High and low correlation coefficients are observed for maize as well as wheat fields. Thus, no real crop-specific pattern between maize and wheat fields is detectable. Considering only time steps with BBCH values below 40 (sparse to medium vegetation cover), the correlation coefficient of the wheat fields increases significantly due to lower vegetation cover. Only one wheat field remains with a correlation coefficient of 0.22, whereas the other test

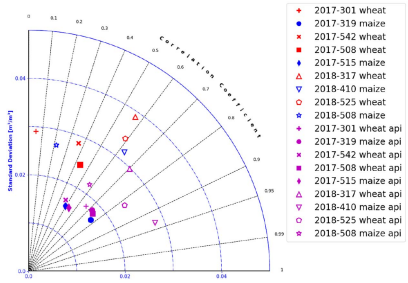

Fig. 15. Standard deviation and correlation coefficient of downscaled and in-situ soil moisture values (red/blue represents wheat/maize; filled/nonfilled represents 2017/2018) as well as RADOLAN API and in-situ values (magenta), for the entire investigation period of 2017 and 2018.

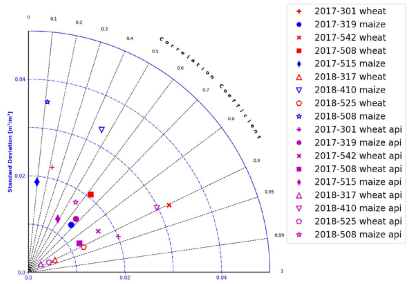

Fig. 16. Standard deviation and correlation coefficient of downscaled and in-situ soil moisture values (red/blue represents wheat/maize; filled/nonfilled represents 2017/2018) as well as RADOLAN API and in-situ value (magenta), for the time period with BBCH values lower than 40 (tillering and stem elongation).

fields, with crop type wheat, show values of up to 0.91. For all maize fields, the correlation coefficient of the RT retrieved soil moisture is dropping compared to the entire time series. Maize fields of 2017 (blue filled icon) show a significantly lower standard deviation for the entire time series as well as for the time series with BBCH values lower than 40 (Figs. 15 and 16) compared to maize fields of 2018 (blue nonfilled icon). However, for the time series with BBCH values higher than 39 (Fig. 17), the standard deviation of all maize fields (blue icons) is similar. Comparing the RADOLAN API and RT retrieved soil moisture results predominantly a lower standard deviation is observed for the RADOLAN API. This is expected as the RADAOLAN API has a lower resolution. Furthermore, the RADOLAN API generally shows better correlation with the in-situ data. It is suspected that this is due to the lower resolution. Through spatial aggregation, it is often observed that soil moisture estimates tend to have a better correlation with in-situ data since local variation and measurement noise are smoothed out.

Fig. 18 shows the downscaled soil moisture pattern of the test site from the end of May to the beginning of June 2017. Fig. 18(f) presents the soil moisture distribution and the precipitation measurements of two meteorological stations (for location relative to the test site, see Fig. 1) for the 29th of May until the 6th of June. A precipitation event occurred on May 30th after the Sentinel-1 overflight. Hence, the precipitation event is not visible in the downscaled soil moisture image [Fig. 18(a)]. Moisture patterns of May 31st indicate higher values for the northern part and almost no soil moisture change in the southern part of the test

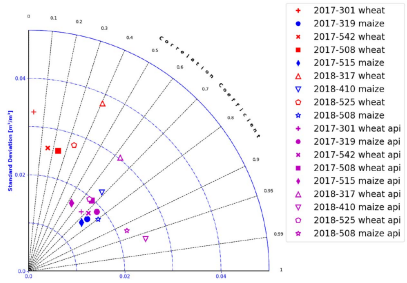

Fig. 17. Standard deviation and correlation coefficient of downscaled and in-situ soil moisture values (red/blue represents wheat/maize; filled/nonfilled represents 2017/2018) as well as RADOLAN API and in-situ value (magenta), for the time period with BBCH values higher than 39 (heading, flowering, fruit development and ripening).

site. This behavior can be explained by the observations at the meteorological stations, where high precipitation was measured at Eichenried (latitude 48.27°) and low to no precipitation was measured southward at Grub (latitude 48.17°). With almost no precipitation between June 1st and 3rd, a conversion of the northern and southern soil moisture values is visible in Fig. 18(c). Another spatially distributed precipitation event occurred on June 4th, with marginal soil moisture changes in the southeast and high changes for the rest of the test area [Fig. 18(d)]. Similar to the situation on June 30th, 2017, the meteorological stations show the same behavior. After two days of precipitation (June 5th and 6th) within the entire test site area, a homogeneous soil moisture pattern with high moisture values is illustrated in Fig. 18(e). The downscaled soil moisture distribution of the test site and the measured precipitation at stations Eichenried and Grub are shown for April to July 2017 in Fig. 19. A comparison of soil moisture changes of the downscaled soil moisture product and the measured precipitation measurements reveal a high alignment of dry-down phases and precipitation events within the data.

Exemplary for the time period of July 19th to 24th of 2018, Fig. 20 illustrates the drying process on the field scale of the MNI test site. Low to no precipitation was measured between July 18 and 20 [Fig. 20(e)]. The precipitation events on July 21st and 22nd are clearly visible by comparing the downscaled soil moisture patterns of July 19th [Fig. 20(a)] and 22nd [Fig. 20(b)]. With almost no precipitation from July 23rd to 26th, the downscaled drying process within the test area can be seen by comparing Fig. 20(b)–(d) and by looking at the soil moisture distribution of July 22nd to 24th in Fig. 20(e). Furthermore, comparing Fig. 20(e) top (downscaled soil moisture distribution) and bottom (precipitation at stations Eichenried and Grub) dry-down phases and precipitation events are mapped very well in the downscaled soil moisture distribution of the test site.

V. Discussion

Continuous, high-resolution, large scale monitoring of a variable like soil moisture with its high spatial and temporal variability is challenging. Current operationally retrieved soil moisture products do not fulfill the demand for temporal and spatial

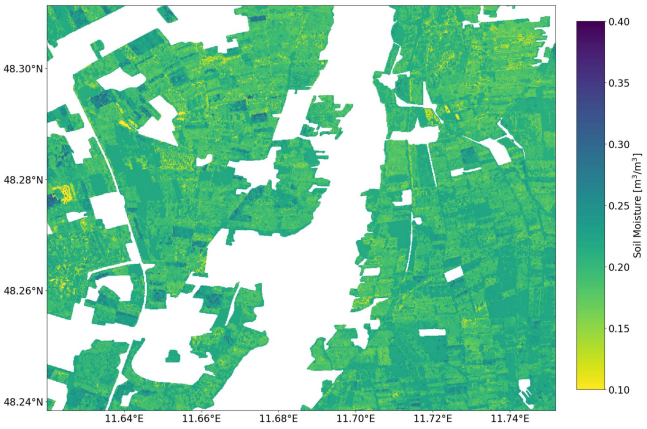

(a) 30th May 2017

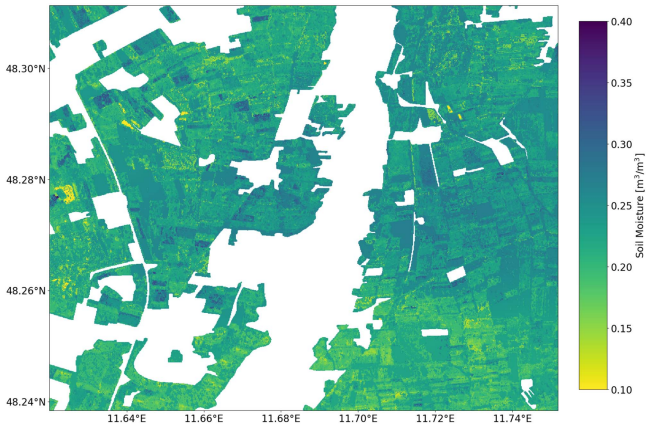

(b) 31st May 2017

(c) 3rd June 2017

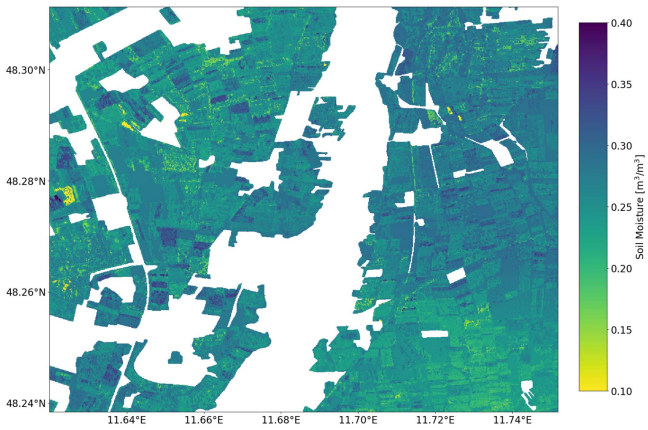

(d) 4th June 2017

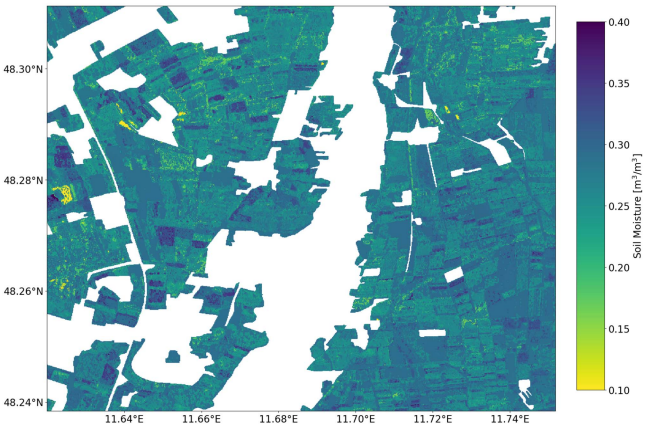

(e) 6th June 2017

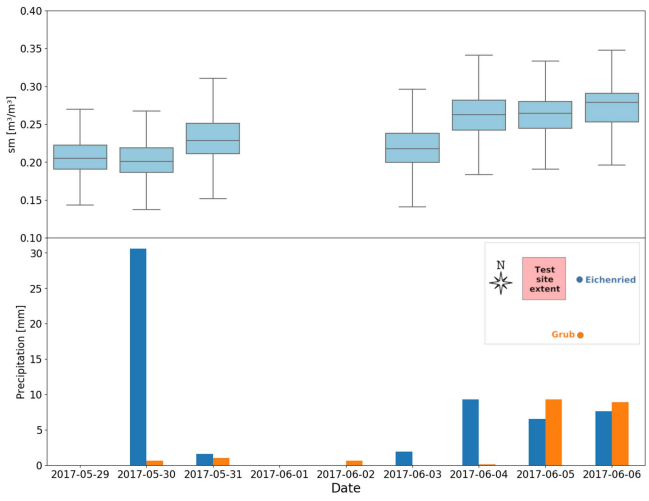

(f) Downscaled soil moisture distribution and measured precipitation events from May 29th to June 6th of 2017

Fig. 18. Downscaled soil moisture pattern of the test site for (a) May 30th, (b) May 31st, and (c) June 3rd, (d) June 4th, and (e) June 6th of 2017. Downscaled soil moisture distribution and measured precipitation events of meteorological stations Eichenried and Grub (f).

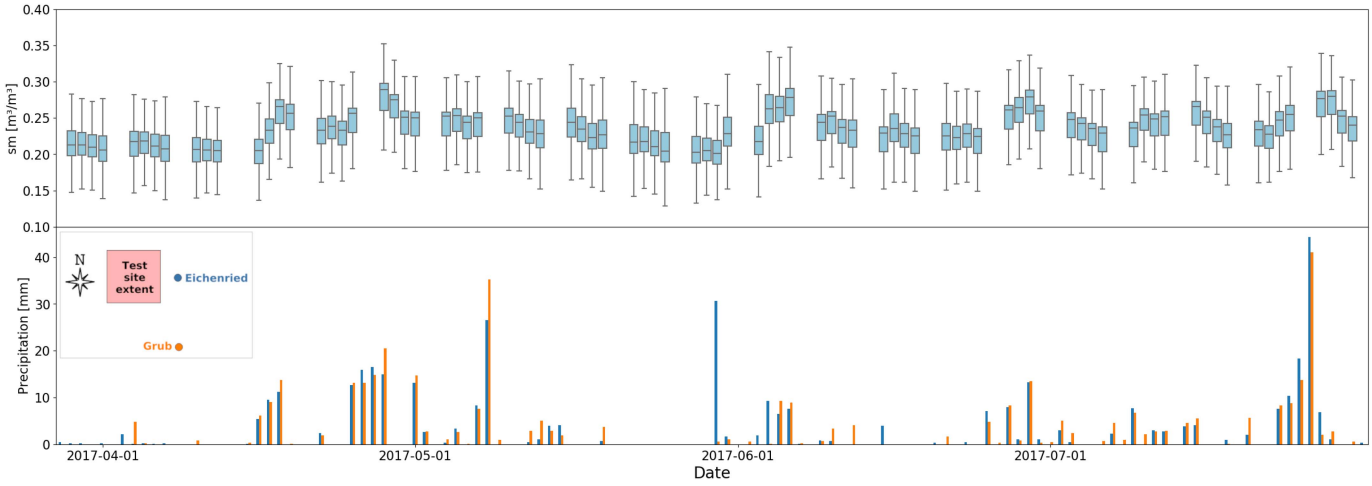

Fig. 19. Downscaled soil moisture distribution (top) and measured precipitation events of meteorological stations Eichenried and Grub (bottom) from April to July 2017.

resolution for smart farming operations [68]. With the Sentinel satellites in orbit, remote sensing data with suitable high spatio-temporal resolution is available for further investigations of soil moisture retrieval approaches. Sentinel-1 (SAR) and Sentinel-2 (optical spectrometer) provide information with a spatial resolution of 10 m (Sentinel-1) and 10–6 m (Sentinel-2), respectively. Sentinel-1 and Sentinel-2 provide images over the same area with the same viewing angle every 6 or 5 days, respectively. The number of usable images from Sentinel-2 decreases when considering cloud cover. For the MNI test site, Sentinel-2 provides a usable image approximately every 10 days. A special challenge however results from a change in the Sentinel-1 observation geometry, namely, modeling the radar backscatter response in conjunction with the associated soil moisture value. Other high resolution soil moisture approaches of Baghdadi et al. [47], El Hajj et al. [19], or Nativel et al. [69] solely use Sentinel-1 images with similar incidence angle. Although, in theory they might be applicable to handle incidence angle changes, [60] has shown that the incidence angle implementation within common RT models (WCM, SSRT) are not sophisticated enough to handle incidence angle changes within one time series. Thus, either each incidence angle needs to be calculated as a separate time series or as we proposed some changes need to be applied. Although more observations (different observation geometries) might be available (depending on the location of the test area) most studies show only a time series based on the Sentinel-1A and Sentinel-1B 6-day repeat cycle. In respect to Sentinel-1A and Sentinel-1B it has to be mentioned that, Sentinel-1B was retired in December 2021 and does not provide images anymore. Nevertheless, the two satellite system should be restored with the planned launch of Sentinel-1C end of 2024. This study proposes a RTM based soil moisture downscaling method that allows for all available Sentinel-1 images (varying viewing angles) to be used, and thus a temporal resolution for the MNI test site of 1.5 days can be archived. However, it has to be mentioned that the soil moisture retrieval quality is also effected by the incidence angle. A study of Bazzi et al. [70] investigated the effect of the incidence angle on soil moisture retrievals from Sentinel-1 and found that lower incidence angle were more suitable than higher ones. With such high spatio-temporal resolution, the results provide an almost daily overview of soil wetting and drying. Furthermore, a differentiation on the field scale is possible in contrast to the medium resolution soil moisture input data. But besides different field scale soil moisture levels, unique differentiated soil moisture patterns due to spatially scattered rain events are also captured (Fig. 20). Nevertheless, as Sentinel-1 images are snapshots of a specific acquisition time, a discrete and noncontinuous time series is produced. A rain event which might occur slightly after the Sentinel-1 overpass is only captured by the follow-on overpass.

The literature shows, that a relationship between the b-parameter and VWC is often used to parameterize vegetation attenuation (VOD) [57], [71], [72]. Furthermore, research of Togliatti et al. [58] indicated that the b-parameter is changing during the growing season. To account for changes in the growing season, the b-parameter was adapted by using normalized VWC information (13) and (16). In previous studies [20], [60], LAI, in combination with an emprical parameter similar to b were used to describe the vegetation status. It was found that the retrieval algorithm had problems deriving good soil moisture estimates for later vegetation stages. Since the used RT-models were not able to reproduce the backscatter increase during later vegetation stages seen in the Sentinel-1 data, LAI with its saturation in later vegetation stages was suspected to be part of the problem. By changing the vegetation descriptor from LAI to VWC, the retrieval algorithm produced better soil moisture results, but did not resolve the backscatter mismatch between the RT-model and the observed Sentinel-1. However, by implementing the proposed VWC normalization and thus changing the dependency of b to a more parabolic form, the retrieval results and the mismatch between the RT-model and Sentinel-1 backscatter could be further improved. Furthermore, previous research by Weißet al. [60] has shown that a joint dense Sentinel-1 time series (all available images disregarding incidence angle changes) is usable within RTMs if considering a correction of the transmissivity term T based on the incidence

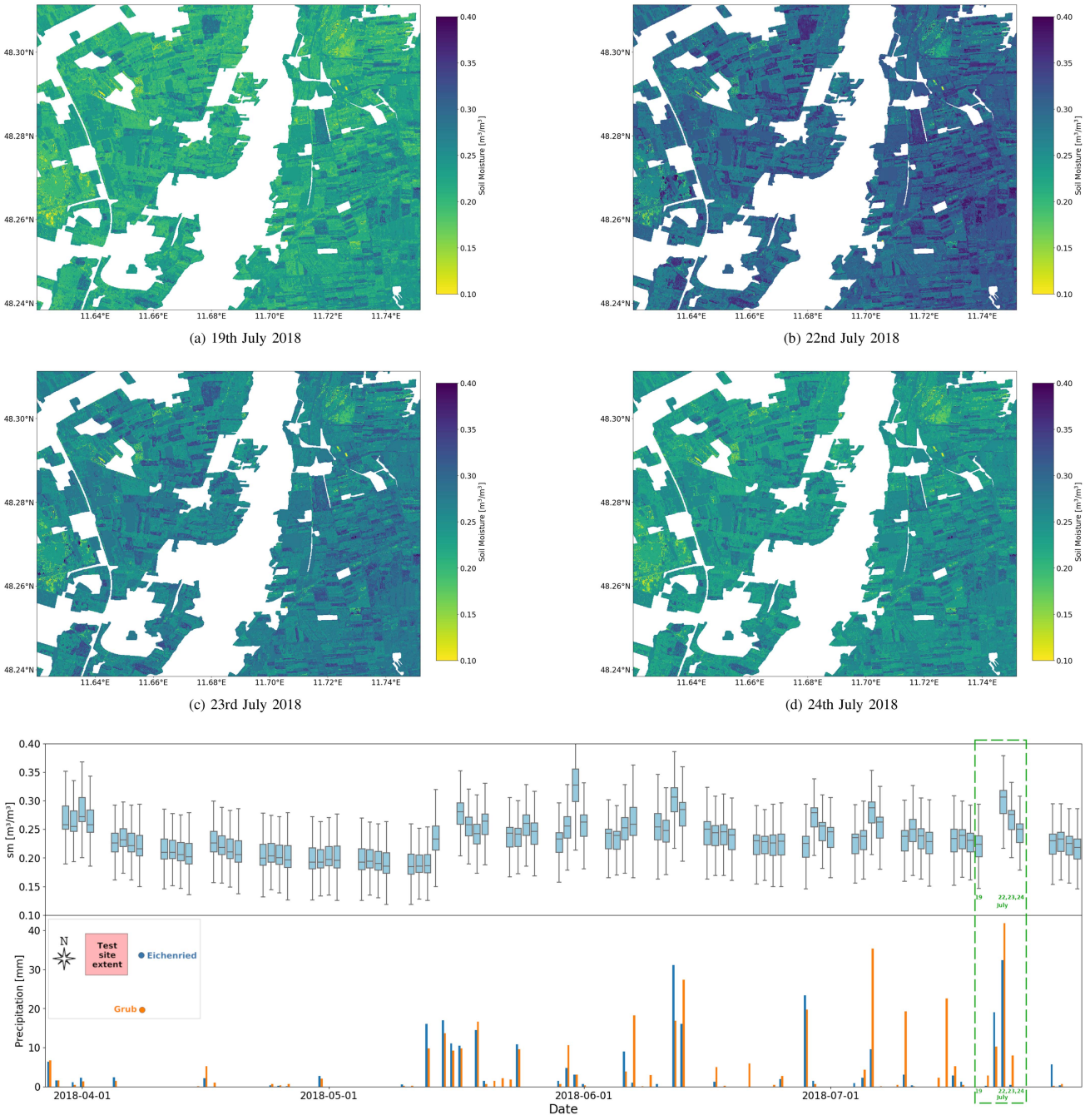

(a) 19th July 2018

(b) 22nd July 2018

(c) 23rd July 2018

(d) 24th July 2018

(e) Downscaled soil moisture distribution and measured precipitation events from April to July 2018. Green box indicate the time period (19-24 July) shown in subfigures a-d.

Fig. 20. Downscaled soil moisture pattern of the test site for (a) July 19th, (b) 22nd, (c) 23rd, and (d) 24th of 2018. Downscaled soil moisture distribution and measured precipitation events of meteorological stations Eichenried and Grub (e).

angle of Sentinel-1. Therefore, different starting points for parameter b based on the incidence angle were used. The VWC, representing the other important input parameter describing the vegetation state, can be derived by crop type specific empirical functions from optical sensors (Sentinel-2), as shown by Maggioni et al. [62], Cosh et al. [73], or Gao et al. [39]. But, as field scale crop type information is often not available on large scales, an empirical function for wheat, the worldwide most widely cultivated crop [74], was used for the entire test site. Although the applied wheat equation may not seem suitable to derive VWC for mutliple crop types, the calculation of an appropriate temporal VWC evolution during the growing season was possible and tested during algorithm development. The ubRMSE values on field scale for different wheat and maize fields range between 0.032 m^3/m^3 and 0.053 m^3/m^3 with a mean ubRMSE for the entire test site of 0.045 m^3/m^3 (2017) and 0.037 m^3/m^3 (2018). It is very probable that the methodology design and thus the modification of the b parameter and its temporal guidance through VWC^{norm} is what produced these good results for the maize fields.

Our results show a similar accuracy in terms of ubRMSE as other high resolution approaches from Tao et al. [75] (0.060 to 0.039 m^3/m^3), El Hajj et al. [19] (0.097 to 0.040 m^3/m^3), Ma et al. [32] (0.078 to 0.039 m^3/m^3) or Mengen et al. [76] (0.063 m^3/m^3). Furthermore, compared with the abovementioned studies, our method provides the highest temporal resolution with almost daily updates for soil moisture values.

A. Transferability

The proposed method is purely based on publicly available information, which can operationally be derived from remote sensing sensors like Sentinel-1, Sentinel-2, or the weather radar network RADOLAN. The applied RTM (Oh04 and SSRT) needs radar backscatter, VWC, and the starting value of the parameter b' (temporal evolution is coupled to VWC) as input data. Specific information about soil composition is not necessary. For VWC calculation, the literature offers different approaches, which are mostly based on spectral information provided by optical sensors like Sentinel-2 or MODIS [62], [73]. Unfortunately, different equations for different crop types are needed to accurately retrieve VWC in absolute terms [39]. Therefore also current crop type information is required. But with the proposed approach (relationship between VWC^{norm} and b), the absolute value of VWC is not as important as the temporal dynamics of VWC during the vegetation growing period. Thus, for simplicity reasons, VWC is calculated using an empirical function suitable for wheat regardless of the crop type. Our study shows, that, although VWC calculation for maize fields is based on the wheat equation, reasonable soil moisture time series patterns (ubRMSE range between 0.032 and 0.053 m^3/m^3) for wheat and maize fields are retrieved. Due to the normalization of VWC, the actual temporal dynamic seems to be more important than the absolute value. This allows the approach to be applied on maize and wheat fields without specific crop type information if the temporal dynamic of VWC is matched. The transferability of the proposed method compared to other approaches from Kim and Liao [77] or Huang et al. [16] thereby is greatly enhanced, due to a lack of specific crop information on field basis for most parts of the world.

Another important input parameter of our study is a soil moisture proxy with medium resolution (1 km × 1 km), which represents the basis for the downscaling efforts. The utilized RADOLAN API product's hourly resolution makes it an excellent prior dataset, however it only covers the spatial domain of Germany. Nevertheless, Ramsauer and Marzahn [78] recently published the global soil moisture product equivalent based on GPM precipitation data (GPM_API). Furthermore, for global use, soil moisture products with resolution from 25 km down to 1 km [11], [79] exist and can be used as soil moisture proxy instead of the RADOLAN based data. In addition, other countries like Poland with POLRAD [80], Switzerland with CombiPrecip [81], or the USA with NEXRAD [82] provide similar information, like the German RADOLAN network. In summary, the proposed approach qualifies for high transferability to be applied to other regions due to its limited set of input variables (VV-polarized backscatter, VWC, and medium resolution soil moisture proxy), which all are provided or can be derived from operational remote sensing sensors.

B. Limitations, Improvements, and Usage

The possible transferability of the approach was theoretically stated in Section V-A, but has to be proven by applying the method to other regions. Furthermore, because of the lack of in-situ measurements for other crop types, only the accuracy of the soil moisture results for wheat and maize fields could be validated in this study. Nevertheless, maize and wheat already account for 65% of the world's cereal production [83]. However, due to our approach (use of time variant b parameter which is normalized by VWC), we found that the evolution of VWC is more important than the absolute values for VWC. We do not expect, that the absolute VWC values of empirical equation defined for wheat will fit other crops like rapeseed or soybean, but as the VWC is based on the optical NDWI index an increase of VWC during the early growing season and an decrease during the drying phase should be matched for all summer cultivated plants. However, this has to be proven with in-situ data. Thus, summarizing the next research focus will be the usage of the method in other regions as well as testing different medium resolution soil moisture products.

One advantage of using microwave data is its penetration capabilities through vegetation cover, and thus the possible retrieval of information about soil moisture conditions under vegetation [84]. The penetration depth of electromagnetic waves into the canopy depends on frequency, polarization, and incidence angle [85]. C-band data is able to penetrate vegetation cover, but with a combination of shallow incidence angles and high vegetation cover (e.g., fully developed maize plants), the backscattering signal of the soil might be very low [85], [86]. For high incidence angles, Joseph et al. [87] and El Hajj et al. [33] showed that even at the biomass peak of maize fields, C-band microwaves were sensitive to soil moisture. They conclude that soil moisture sensitivity is given due to significant soil-vegetation scattering contributions. On the other hand, in case of a full developed wheat field, the penetration of C-band into the canopy was found limited [33]. During certain growing stages (booting, heading, flowering, fruit development) where wheat plants contain a lot of canopy water, the penetration of C-band is highly dampened [60]. However, for later wheat growing stages (ripening) the sensitivity of C-band to the soil and soil moisture does increase [88], [89]. The sensitivity increase can be attributed to the loss of canopy water which makes the vegetation layer more transparent for microwaves. We see the effect of changing C-band sensitivity during the growing season of wheat by comparing Figs. 16 and 17. The correlation coefficient drops significantly between the first and the second half of the growing season. In addition, the ubRMSE in Table IV for wheat fields shows better results for BBCH<40 than BBCH>39. But, the ubRMSE values for BBCH>39 are still in an acceptable range of 0.032 to 0.048 m^3/m^3. Thus, we suspect that during growing stages like heading and flowering the proposed approach relies more on the soil moisture prior information. Therefore, in case of high vegetation cover, the application of radar sensors with lower frequencies, e.g., L-band might increase the accuracy of the retrieval results due to its higher vegetation penetration [90], especially at low incidence angles. Unfortunately, no operational L-band dataset with high

temporal and spatial resolution is currently available, but the NISAR mission of NASA is upcoming [91].

Promising results for large scale provision of crop type information are shown with optical data by Inglada et al. [92] and with combined optical and microwave data by Orynbaikyzy et al. [93], Ofori-Ampofo et al. [94], and Blickensdörfer et al. [95]. But as crop types might differ every year, and distinction levels might not exceed a differentiation of summer and winter crops [92], operational application might be difficult on global scales.

Another limitation of the proposed methodology in its current status is that the normalization of VWC is based on maximum and minimum values. This means that in its current status the method can only be applied after the growing period. However, additional crop specific a priori data from previous years might be usable to apply the methodology already during the growing period. Nevertheless, this needs more investigation. If the abovementioned limitation can be overcome, then we will be another step further towards providing high temporal and spatial soil moisture information for applications in terms of smart farming decisions [8] and improved crop yield estimations [96]. In areas with irrigation, high spatio-temporal information about soil moisture has the potential to improve water usage on a local to regional scale [97]. Furthermore, spatially distributed soil moisture information helps by minimizing fertilizer usage [7], and thus reducing pollution of surface and groundwater resources [98]. In addition, soil erosion often depends on local conditions, which means that for soil erosion modeling and agricultural adaptation strategies, high spatio-temporal soil moisture information is vital [68].

VI. Conclusion

A soil moisture time series product with medium spatial resolution (RADOLAN API 1 km $\times$ 1 km) was downscaled to field scale by applying an adapted microwave RTM. For model input, high spatio-temporal VV-polarized backscatter (Sentinel-1; 10 m $\times$ 10 m) and VWC information derived from optical sensors (Sentinel-2; 20 m $\times$ 20 m) were used. For parameters like soil roughness, which were considered static over the growing season, suitable literature values were chosen [60]. The retrieved high spatio-temporal distributed soil moisture information was further validated with in-situ measurements (MNI test site in Bavaria, Germany) of wheat and maize fields during the vegetation growing periods of 2017 and 2018.

A validation of soil moisture with in-situ measurements of several fields reveals good agreement with a mean ubRMSE of 0.045 m^3/m^3 and 0.037 m^3/m^3 for the years 2017 and 2018, respectively. Furthermore, the downscaled soil moisture covers a broad range of values from 0.05 m^3/m^3 to 0.4 m^3/m^3. In addition, spatial patterns from precipitation events and drying behavior within the test site are clearly visible within the downscaled soil moisture images. Overall, it is demonstrated that with a small and well selected set of input parameters which are publicly provided by different optical and microwave remote sensing sensors, the generation of high spatio-temporal distributed soil moisture patterns is feasible by using RTM-based downscaling over the investigated agricultural fields.

One advantage of the proposed methodology is the usage of all available Sentinel-1 images regardless of the observation geometry which lead to changes of the radar backscatter response. Thus, the temporal resolution constraint due to the Sentinel-1A and Sentinel-1B 6-day repeat cycle (same observation geometry, same orbit, same incidence angle, same observation time) is overcome and in case of the MNI test site a 1.5 d temporal resolution is archived. Unfortunately, right now only Sentinel-1A provides images as Sentinel-1B had a power supply issue and was retired in December 2021. Nevertheless, the upcoming Sentinel-1C will hopefully restore the two satellite system before the end of 2024.

Another advantage of the proposed methodology is its high transferability to other regions, as the used retrieval algorithm relies only on information that can be systematically retrieved with existing global operational satellites (Sentinel-1 and Sentinel-2) and a coarse to medium resolution soil moisture prior. A comparison of different medium and low resolution soil moisture proxy as prior and the application of the methods on other test sites is needed to further explore and optimize the quality of the spatio-temporal soil moisture estimates at decameter resolution. Possible pitfalls of the transferability of this and other high resolution soil moisture retrieval approaches might be uncertainties due to landscape heterogeneity (soil properties, crop types, vegetation stages). Thus, in order to further reduce uncertainties, opportunities may arise by including site specific auxiliary information (soil texture or crop type) within the proposed downscaling scheme. Hence, the approach offers multiple opportunities for enhancement by including additional information which are or will be provided in the future by remote sensing sensors and techniques.

Acknowledgment

The author Thomas Weißis would like to thank Alexander Läw († 2. July 2017) for the inspiration, ideas, and support that he has given.

References

[1] H. McNairn, A. Merzouki, A. Pacheco, and J. Fitzmaurice, "Monitoring soil moisture to support risk reduction for the agriculture sector using RADARSAT-2," *IEEE J. Sel. Topics Appl. Earth Observ. Remote Sens.*, vol. 5, no. 3, pp. 824–834, Jun. 2012.

[2] R. Hollmann et al., "The ESA climate change initiative: Satellite data records for essential climate variables," *Bull. Amer. Meteorological Soc.*, vol. 94, no. 10, pp. 1541–1552, Mar. 2013, doi: 10.1175/BAMS-D-11-00254.1.

[3] L. Brocca, L. Ciabatta, C. Massari, S. Camici, and A. Tarpanelli, "Soil moisture for hydrological applications: Open questions and new opportunities," *Water*, vol. 9, no. 2, Feb. 2017, Art. no. 140. [Online]. Available: https://www.mdpi.com/2073-4441/9/2/140

[4] L. Brocca, F. Melone, T. Moramarco, and R. Morbidelli, "Spatial-temporal variability of soil moisture and its estimation across scales," *Water Resour. Res.*, vol. 46, no. 2, 2010, Art. no. W02516. [Online]. Available: https://agupubs.onlinelibrary.wiley.com/doi/abs/10.1029/2009WR008016

[5] J. Dari, R. Morbidelli, C. Saltalippi, C. Massari, and L. Brocca, "Spatial-temporal variability of soil moisture: Addressing the monitoring at the catchment scale," *J. Hydrol.*, vol. 570, pp. 436–444, Mar. 2019. [Online]. Available: http://www.sciencedirect.com/science/article/pii/S0022169419300575

[6] N. Sanchez, L. Almendra, J. Plaza, A. González-Zamora, and J. Martínez-Fernández, "Spatial averages of in situ measurements versus remote sensing observations: A soil moisture analysis," *J. Spatial Sci.*, vol. 67, no. 3, pp. 439–454, 2022, doi: 10.1080/14498596.2020.1833769.

[7] J. Peng et al., "Estimation and evaluation of high-resolution soil moisture from merged model and earth observation data in the Great Britain," *Remote Sens. Environ.*, vol. 264, Oct. 2021, Art. no. 112610. [Online]. Available: https://www.sciencedirect.com/science/article/pii/S0034425721003308

[8] J. Peng, A. Loew, O. Merlin, and N. E. C. Verhoest, "A review of spatial downscaling of satellite remotely sensed soil moisture," *Rev. Geophys.*, vol. 55, no. 2, pp. 341–366, 2017. [Online]. Available: https://onlinelibrary.wiley.com/doi/abs/10.1002/2016RG000543

[9] J. Peng, A. Loew, S. Zhang, J. Wang, and J. Niesel, "Spatial downscaling of satellite soil moisture data using a vegetation temperature condition index," *IEEE Trans. Geosci. Remote Sens.*, vol. 54, no. 1, pp. 558–566, Jan. 2016.

[10] B. Bauer-Marschallinger et al., "Toward global soil moisture monitoring with Sentinel-1: Harnessing assets and overcoming obstacles," *IEEE Trans. Geosci. Remote Sens.*, vol. 57, no. 1, pp. 520–539, Jan. 2019.

[11] N. N. Das et al., "The SMAP and copernicus sentinel 1 A/B microwave active-passive high resolution surface soil moisture product," *Remote Sen/s. Environ.*, vol. 233, Nov. 2019, Art. no. 111380. [Online]. Available: https://www.sciencedirect.com/science/article/pii/S0034425719303992

[12] T. Ramsauer, T. Weiß, and P. Marzahn, "RADOLAN_API - A soil moisture data set derived from weather radar data," Apr. 2021. [Online]. Available: https://zenodo.org/record/4588904

[13] P. Rao, Y. Wang, F. Wang, Y. Liu, X. Wang, and Z. Wang, "Daily soil moisture mapping at 1 km resolution based on SMAP data for desertification areas in northern China," *Earth Syst. Sci. Data*, vol. 14, no. 7, pp. 3053–3073, Jul. 2022. [Online]. Available: https://essd.copernicus.org/articles/14/3053/2022/

[14] T. Jagdhuber, I. Hajnsek, and K. P. Papathanassiou, "Refined soil moisture estimation by means of l-band polarimetry," in *2013 IEEE Int. Geosci. Remote Sens. Symp.- IGARSS*, Jul. 2013, pp. 2325–2328.

[15] S. H. Alemohammad, T. Jagdhuber, M. Moghaddam, and D. Entekhabi, "Soil and vegetation scattering contributions in L-band and P-band polarimetric SAR observations," *IEEE Trans. Geosci. Remote Sens.*, vol. 57, no. 11, pp. 8417–8429, Nov. 2019.

[16] X. Huang, B. Ziniti, M. H. Cosh, M. Reba, J. Wang, and N. Torbick, "Field-scale soil moisture retrieval using PALSAR-2 polarimetric decomposition and machine learning," *Agronomy*, vol. 11, no. 1, Jan. 2021, Art. no. 35. [Online]. Available: https://www.mdpi.com/2073-4395/11/1/35

[17] N. S. Chauhan, S. Miller, and P. Ardanuy, "Spaceborne soil moisture estimation at high resolution: A microwave-optical/IR synergistic approach," *Int. J. Remote Sens.*, vol. 24, no. 22, pp. 4599–4622, Jan. 2003, doi: 10.1080/0143116031000156837.

[18] A. Loew and W. Mauser, "On the disaggregation of passive microwave soil moisture data using a priori knowledge of temporally persistent soil moisture fields," *IEEE Trans. Geosci. Remote Sens.*, vol. 46, no. 3, pp. 819–834, Mar. 2008.

[19] M. El Hajj, N. Baghdadi, M. Zribi, and H. Bazzi, "Synergic use of Sentinel-1 and Sentinel-2 images for operational soil moisture mapping at high spatial resolution over agricultural areas," *Remote Sens.*, vol. 9, no. 12, Dec. 2017, Art. no. 1292. [Online]. Available: https://www.mdpi.com/2072-4292/9/12/1292

[20] T. Weiß, T. Ramsauer, A. Löw, and P. Marzahn, "Evaluation of different radiative transfer models for microwave backscatter estimation of wheat fields," *Remote Sens.*, vol. 12, no. 18, Jan. 2020, Art. no. 3037. [Online]. Available: https://www.mdpi.com/2072-4292/12/18/3037

[21] M. Neelam and B. P. Mohanty, "On the radiative transfer model for soil moisture across space, time and hydro-climates," *Remote Sens.*, vol. 12, no. 16, Jan. 2020, Art. no. 2645. [Online]. Available: https://www.mdpi.com/2072-4292/12/16/2645

[22] M. Owe, R. de Jeu, and J. Walker, "A methodology for surface soil moisture and vegetation optical depth retrieval using the microwave polarization difference index," *IEEE Trans. Geosci. Remote Sens.*, vol. 39, no. 8, pp. 1643–1654, Aug. 2001.

[23] G. J. M. D. Lannoy, R. H. Reichle, and V. R. N. Pauwels, "Global calibration of the GEOS-5 L-band microwave radiative transfer model over nonfrozen land using SMOS observations," *J. Hydrometeorol.*, vol. 14, no. 3, pp. 765–785, Jun. 2013.

[24] Y. Oh, K. Sarabandi, and F. Ulaby, "An empirical model and an inversion technique for radar scattering from bare soil surfaces," *IEEE Trans. Geosci. Remote Sens.*, vol. 30, no. 2, pp. 370–381, Mar. 1992.

[25] Y. Oh, "Quantitative retrieval of soil moisture content and surface roughness from multipolarized radar observations of bare soil surfaces," *IEEE Trans. Geosci. Remote Sens.*, vol. 42, no. 3, pp. 596–601, Mar. 2004.

[26] P. Dubois, J. van Zyl, and T. Engman, "Measuring soil moisture with imaging radars," *IEEE Trans. Geosci. Remote Sens.*, vol. 33, no. 4, pp. 915–926, Jul. 1995.

[27] A. Fung, W. Liu, K. Chen, and M. Tsay, "An improved iem model for bistatic scattering from rough surfaces," *J. Electromagn. Waves Appl.*, vol. 16, no. 5, pp. 689–702, Jan. 2002. [Online]. Available: https://www.tandfonline.com/doi/full/10.1163/156939302X01119

[28] N. Baghdadi et al., "Potential of Sentinel-1 images for estimating the soil roughness over bare agricultural soils," *Water*, vol. 10, no. 2, Feb. 2018, Art. no. 131. [Online]. Available: https://www.mdpi.com/2073-4441/10/2/131

[29] E. P. W. Attema and F. T. Ulaby, "Vegetation modeled as a water cloud," *Radio Sci.*, vol. 13, no. 2, pp. 357–364, Mar. 1978.

[30] R. de Roo, Y. Du, F. Ulaby, and M. Dobson, "A semi-empirical backscattering model at L-band and C-band for a soybean canopy with soil moisture inversion," *IEEE Trans. Geosci. Remote Sens.*, vol. 39, no. 4, pp. 864–872, Apr. 2001.

[31] F. T. Ulaby and D. G. Long, *Microwave Radar and Radiometric Remote Sensing*. Ann Arbor, MI, USA: Univ. Michigan Press, 2014.

[32] C. Ma, X. Li, and M. F. McCabe, "Retrieval of high-resolution soil moisture through combination of Sentinel-1 and Sentinel-2 data," *Remote Sens.*, vol. 12, no. 14, Jan. 2020, Art. no. 2303. [Online]. Available: https://www.mdpi.com/2072-4292/12/14/2303

[33] M. El Hajj, N. Baghdadi, H. Bazzi, and M. Zribi, "Penetration analysis of SAR signals in the C and L bands for wheat, maize, and grasslands," *Remote Sens.*, vol. 11, no. 1, Jan. 2019, Art. no. 31. [Online]. Available: https://www.mdpi.com/2072-4292/11/1/31

[34] H. Bazzi et al., "Detecting irrigation events over semi-arid and temperate climatic areas using Sentinel-1 data: Case of several summer crops," *Agronomy*, vol. 12, no. 11, Nov. 2022, Art. no. 2725. [Online]. Available: https://www.mdpi.com/2073-4395/12/11/2725

[35] T. Meyer et al., "Estimating gravimetric water content of a winter wheat field from L-band vegetation optical depth," *Remote Sens.*, vol. 11, no. 20, Jan. 2019, Art. no. 2353. [Online]. Available: https://www.mdpi.com/2072-4292/11/20/2353

[36] M. H. Cosh et al., "Estimating vegetation water content during the Soil Moisture Active Passive Validation Experiment 2016," *J. Appl. Remote Sens.*, vol. 13, no. 1, Feb. 2019, Art. no. 014516.

[37] F. Frappart et al., "Global monitoring of the vegetation dynamics from the vegetation optical depth (VOD): A review," *Remote Sens.*, vol. 12, no. 18, Jan. 2020, Art. no. 2915. [Online]. Available: https://www.mdpi.com/2072-4292/12/18/2915

[38] E. M. Perry, E. M. Morse-McNabb, J. G. Nuttall, G. J. O'Leary, and R. Clark, "Managing wheat from space: Linking MODIS NDVI and crop models for predicting australian dryland wheat biomass," *IEEE J. Sel. Topics Appl. Earth Observ. Remote Sens.*, vol. 7, no. 9, pp. 3724–3731, Sep. 2014.

[39] Y. Gao, J. P. Walker, M. Allahmoradi, A. Monerris, D. Ryu, and T. J. Jackson, "Optical sensing of vegetation water content: A synthesis study," *IEEE J. Sel. Topics Appl. Earth Observ. Remote Sens.*, vol. 8, no. 4, pp. 1456–1464, Apr. 2015.

[40] X.-P. Song, W. Huang, M. C. Hansen, and P. Potapov, "An evaluation of landsat, Sentinel-2, Sentinel-1 and MODIS data for crop type mapping," *Sci. Remote Sens.*, vol. 3, Jun. 2021, Art. no. 100018. [Online]. Available: https://www.sciencedirect.com/science/article/pii/S2666017221000055

[41] Q. Gao, M. Zribi, M. J. Escorihuela, and N. Baghdadi, "Synergetic use of Sentinel-1 and Sentinel-2 data for soil moisture mapping at 100 m resolution," *Sensors*, vol. 17, no. 9, Sep. 2017, Art. no. 1966. [Online]. Available: https://www.mdpi.com/1424-8220/17/9/1966

[42] F. Mattia et al., "Sentinel-1 & Sentinel-2 for SOIL moisture retrieval at field scale," in *2018 IEEE Int. Geosci. Remote Sens. Symp.*, Jul. 2018, pp. 6143–6146.

[43] M. Wocher, K. Berger, M. Danner, W. Mauser, and T. Hank, "Physically-based retrieval of canopy equivalent water thickness using hyperspectral data," *Remote Sens.*, vol. 10, no. 12, 2018, Art. no. 1924.

[44] M. Danner, K. Berger, M. Wocher, W. Mauser, and T. Hank, "Fitted PROSAIL parameterization of leaf inclinations, water content and brown pigment content for winter wheat and maize canopies," *Remote Sens.*, vol. 11, no. 10, 2019, Art. no. 1150.

[45] T. Weiß and T. Fincke, "SenSARP: A pipeline to pre-process Sentinel-1 SLC data by using ESA SNAP Sentinel-1 toolbox," *J. Open Source Softw.*, vol. 7, no. 69, Jan. 2022, Art. no. 3337. [Online]. Available: https://joss.theoj.org/papers/10.21105/joss.03337

[46] M. El Hajj et al., "Soil moisture retrieval over irrigated grassland using X-band SAR data," *Remote Sens. Environ.*, vol. 176, pp. 202–218, Apr. 2016. [Online]. Available: http://www.sciencedirect.com/science/article/pii/S0034425716300281

[47] N. Baghdadi, M. El Hajj, M. Zribi, and S. Bousbih, "Calibration of the water cloud model at C-band for winter crop fields and grasslands," *Remote Sens.*, vol. 9, no. 9, Sep. 2017, Art. no. 969. [Online]. Available: https://www.mdpi.com/2072-4292/9/9/969

[48] E. Vermote, D. Tanre, J. Deuze, M. Herman, and J.-J. Morcette, "Second simulation of the satellite signal in the solar spectrum, 6S: An overview," *IEEE Trans. Geosci. Remote Sens.*, vol. 35, no. 3, pp. 675–686, May 1997.

[49] R. T. Wilson, "Py6S: A python interface to the 6S radiative transfer model," *Comput. Geosci.*, vol. 51, pp. 166–171, Feb. 2013. [Online]. Available: https://www.sciencedirect.com/science/article/pii/S0098300412002798

[50] T. Ramsauer, T. Weiß, A. Löw, and P. Marzahn, "RADOLAN_API: An hourly soil moisture data set based on weather radar, soil properties and reanalysis temperature data," *Remote Sens.*, vol. 13, no. 9, Jan. 2021, Art. no. 1712. [Online]. Available: https://www.mdpi.com/2072-4292/13/9/1712

[51] H. Bartels, "Projekt RADOLAN. Routineverfahren zur Online-A neichung der Radarniederschlagsdaten mit Hilfe von Automatischen Bodenniederschlagsstationen (Ombrometer)," Deutscher Wetterdienst, Offenbach, Germany, Tech. Rep., 2004.

[52] T. Winterrath et al., "An overview of the new radar-based precipitation climatology of the Deutscher Wetterdienst–data, methods, products," in *Proc. 11th Int. Workshop Precipitation Urban Areas Rainfall Monit. Modelling Forecasting Urban Environ.*, ETH Zurich, Institute of Environmental Engineering, 2019, pp. 132–137. [Online]. Available: https://www.research-collection.ethz.ch/handle/20.500.11850/347607

[53] M. A. Kohler and R. K. Linsley, *Predicting the Runoff from Storm Rainfall* vol. 30, US Department of Commerce, Weather Bureau, 1951.

[54] T. Hengl et al., "SoilGrids250 m: Global gridded soil information based on machine learning," *PLoS One*, vol. 12, no. 2, Feb. 2017, Art. no. e0169748, doi: 10.1371/journal.pone.0169748.

[55] European Environment Agency, "CORINE land cover 2018," 2018. [Online]. Available: https://land.copernicus.eu/pan-european/corine-land-cover/clc2018

[56] Y. Oh, K. Sarabandi, and F. Ulaby, "Semi-empirical model of the ensemble-averaged differential mueller matrix for microwave backscattering from bare soil surfaces," *IEEE Trans. Geosci. Remote Sens.*, vol. 40, no. 6, pp. 1348–1355, Jun. 2002.

[57] T. J. Jackson and T. J. Schmugge, "Vegetation effects on the microwave emission of soils," *Remote Sens. Environ.*, vol. 36, no. 3, pp. 203–212, Jun. 1991. [Online]. Available: https://www.sciencedirect.com/science/article/pii/003442579190057D

[58] K. Togliatti, C. Lewis-Beck, V. A. Walker, T. Hartman, A. VanLoocke, and B. K. Hornbuckle, "The B-parameter relating L-VOD to satellite-scale crop plant water may not be constant over a growing season," in *2021 IEEE Int. Geosci. Remote Sens. Symp. IGARSS*, Jul. 2021, pp. 6857–6860.

[59] T. Hartman, R. Cirone, K. Togliatti, B. K. Hornbuckle, and A. VanLoocke, "A spatial and temporal evaluation of the SMAP cropland b-parameter across the U.S. Corn Belt," *Remote Sens. Environ.*, vol. 297, Nov. 2023, Art. no. 113752. [Online]. Available: https://www.sciencedirect.com/science/article/pii/S0034425723003036

[60] T. Weiß, T. Ramsauer, T. Jagdhuber, A. Löw, and P. Marzahn, "Sentinel-1 backscatter analysis and radiative transfer modeling of dense winter wheat time series," *Remote Sens.*, vol. 13, no. 12, Jan. 2021, Art. no. 2320. [Online]. Available: https://www.mdpi.com/2072-4292/13/12/2320

[61] T. J. Jackson et al., "Vegetation water content mapping using landsat data derived normalized difference water index for corn and soybeans," *Remote Sens. Environ.*, vol. 92, no. 4, pp. 475–482, Sep. 2004. [Online]. Available: https://www.sciencedirect.com/science/article/pii/S0034425703003353

[62] V. Maggioni et al., "A multi-sensor approach for high resolution airborne soil moisture mapping," in *Proc. 30th Hydrol. Water Resour. Symp.*, 2006, pp. 297–302.

[63] H. Lu, T. Koike, H. Tsutsui, and H. Fujii, "Monitoring vegetation water content by using optical vegetation index and microwave vegetation index: Field experiments and applications," in *2011 IEEE Int. Geosci. Remote Sens. Symp.*, Jul. 2011, pp. 2468–2471.

[64] SciPy Community, "SciPy: Open source scientific tools for Python," manual, 2024. [Online]. Available: https://docs.scipy.org/doc/scipy/reference/optimize.minimize-lbfgsb.html#optimize-minimize-lbfgsb

[65] P. Lewis et al., "An earth observation land data assimilation system (EO-LDAS)," *Remote Sens. Environ.*, vol. 120, pp. 219–235, May 2012. [Online]. Available: https://www.sciencedirect.com/science/article/pii/S0034425712000788

[66] T. Quaife et al., "Synergistic retrievals of leaf area index and soil moisture from Sentinel-1 and Sentinel-2," *Int. J. Image Data Fusion*, vol. 14, no. 3, pp. 225–242, Dec. 2022, doi: 10.1080/19479832.2022.2149629.

[67] U. Meier et al., "The BBCH system to coding the phenological growth stages of plants–history and publications," *J. für Kulturpflanzen*, vol. 61, no. 2, pp. 41–52, Feb. 2009. [Online]. Available: https://ojs.openagrar.de/index.php/Kulturpflanzenjournal/article/view/12142

[68] J. Peng et al., "A roadmap for high-resolution satellite soil moisture applications–confronting product characteristics with user requirements," *Remote Sens. Environ.*, vol. 252, Jan. 2021, Art. no. 112162. [Online]. Available: https://www.sciencedirect.com/science/article/pii/S0034425720305356

[69] S. Nativel et al., "Hybrid methodology using Sentinel-1/Sentinel-2 for soil moisture estimation," *Remote Sens.*, vol. 14, no. 10, Jan. 2022, Art. no. 2434. [Online]. Available: https://www.mdpi.com/2072-4292/14/10/2434

[70] H. Bazzi et al., "Retrieving soil moisture from Sentinel-1: Limitations over certain crops and sensitivity to the first soil thin layer," *Water*, vol. 16, no. 1, Jan. 2024, Art. no. 40. [Online]. Available: https://www.mdpi.com/2073-4441/16/1/40

[71] A. G. Konings, M. Piles, K. Rötzer, K. A. McColl, S. K. Chan, and D. Entekhabi, "Vegetation optical depth and scattering albedo retrieval using time series of dual-polarized L-band radiometer observations," *Remote Sens. Environ.*, vol. 172, pp. 178–189, Jan. 2016. [Online]. Available: https://www.sciencedirect.com/science/article/pii/S003442571530198X

[72] T. Jagdhuber et al., "Physics-based modeling of active-passive microwave covariations for geophysical retrievals," in *2018 IEEE Int. Geosci. Remote Sens. Symp.*, Jul. 2018, pp. 250–253.

[73] M. H. Cosh, J. Tao, T. J. Jackson, L. McKee, and P. E. O'Neill, "Vegetation water content mapping in a diverse agricultural landscape: National Airborne Field Experiment 2006," *J. Appl. Remote Sens.*, vol. 4, no. 1, 2010, Art. no. 043532. [Online]. Available: https://handle.nal.usda.gov/10113/56319

[74] O. Erenstein, M. Jaleta, K. A. Mottaleb, K. Sonder, J. Donovan, and H.-J. Braun, "Global Trends in Wheat Production, Consumption and Trade," in *Wheat Improvement: Food Security in a Changing Climate*, Cham, Switzerland: Springer International Publishing, 2022, pp. 47–66.

[75] L. Tao, G. Wang, X. Chen, J. Li, and Q. Cai, "Estimation of soil moisture using a vegetation scattering model in wheat fields," *J. Appl. Remote Sens.*, vol. 13, no. 4, Oct. 2019, Art. no. 044503.

[76] D. Mengen, T. Jagdhuber, A. Balenzano, F. Mattia, H. Vereecken, and C. Montzka, "High spatial and temporal soil moisture retrieval in agricultural areas using multi-orbit and vegetation adapted Sentinel-1 SAR time series," *Remote Sens.*, vol. 15, no. 9, Jan. 2023, Art. no. 2282. [Online]. Available: https://www.mdpi.com/2072-4292/15/9/2282

[77] S.-B. Kim and T.-H. Liao, "Robust retrieval of soil moisture at field scale across wide-ranging SAR incidence angles for soybean, wheat, forage, oat and grass," *Remote Sens. Environ.*, vol. 266, Dec. 2021, Art. no. 112712. [Online]. Available: https://www.sciencedirect.com/science/article/pii/S0034425721004326

[78] T. Ramsauer and P. Marzahn, "Global soil moisture estimation based on GPM IMERG data using a site specific adjusted antecedent precipitation index," *Int. J. Remote Sens.*, vol. 44, no. 2, pp. 542–566, Jan. 2023, doi: 10.1080/01431161.2022.2162351.

[79] G. Portal et al., "Assessment of multi-scale SMOS and SMAP soil moisture products across the iberian peninsula," *Remote Sens.*, vol. 12, no. 3, Jan. 2020, Art. no. 570. [Online]. Available: https://www.mdpi.com/2072-4292/12/3/570

[80] J. Szturc, K. Osródka, A. Jurczyk, and L. Jelonek, "Concept of dealing with uncertainty in radar-based data for hydrological purpose," *Natural Hazards Earth Syst. Sci.*, vol. 8, no. 2, pp. 267–279, Mar. 2008. [Online]. Available: https://hal.archives-ouvertes.fr/hal-00299505

[81] Y. Barton, I. V. Sideris, T. H. Raupach, M. Gabella, U. Germann, and O. Martius, "A multi-year assessment of sub-hourly gridded precipitation for Switzerland based on a blended radar–Rain-gauge dataset," *Int. J. Climatol.*, vol. 40, no. 12, pp. 5208–5222, 2020. [Online]. Available: https://onlinelibrary.wiley.com/doi/abs/10.1002/joc.6514

[82] G. Schoener and M. C. Stone, "Monitoring soil moisture at the catchment scale–A novel approach combining antecedent precipitation index and radar-derived rainfall data," *J. Hydrol.*, vol. 589, Oct. 2020, Art. no. 125155. [Online]. Available: https://www.sciencedirect.com/science/article/pii/S0022169420306156

[83] O. Erenstein, J. Chamberlin, and K. Sonder, "Estimating the global number and distribution of maize and wheat farms," *Glob. Food Secur.*, vol. 30, Sep. 2021, Art. no. 100558. [Online]. Available: https://www.sciencedirect.com/science/article/pii/S2211912421000675

[84] T. Jagdhuber, "Soil parameter retrieval under vegetation cover using SAR polarimetry," PhD Thesis, Fac. Math. Nat. Sci., Univ. Potsdam, Potsdam, Germany, 2012.

[85] H.S. Srivastava, P. Patel, and R. R. Navalgund, "How far SAR has fulfilled its expectation for soil moisture retrieval," in *Microwave Remote Sensing of the Atmosphere and Environment V*, vol. 6410. Bellingham, WA, USA: SPIE, Dec. 2006, Art. no. 641001. [Online]. Available: https://www.spiedigitallibrary.org/conference-proceedings-of-spie/6410/641001/How-far-SAR-has-fulfilled-its-expectation-for-soil-moisture/10.1117/12.693946.full

[86] J. Bouchat, E. Tronquo, A. Orban, X. Neyt, N. E. C. Verhoest, and P. Defourny, "Green area index and soil moisture retrieval in maize fields using multi-polarized C- and L-band SAR data and the water cloud model," *Remote Sens.*, vol. 14, no. 10, Jan. 2022, Art. no. 2496. [Online]. Available: https://www.mdpi.com/2072-4292/14/10/2496

[87] A. T. Joseph, R. van der Velde, P. E. O'Neill, R. Lang, and T. Gish, "Effects of corn on c- and l-band radar backscatter: A correction method for soil moisture retrieval," *Remote Sens. Environ.*, vol. 114, no. 11, pp. 2417–2430, Nov. 2010. [Online]. Available: https://www.sciencedirect.com/science/article/pii/S0034425710001641

[88] L. He, L. Tong, Y. Li, Y. Chen, L. Tan, and C. Guo, "Polarimetric analysis of radar backscatter from ground-based scatterometers and wheat biomass monitoring with advanced synthetic aperture radar images," *J. Appl. Remote Sens.*, vol. 10, no. 2, Apr. 2016, Art. no. 026008.

[89] F. Mattia et al., "Multitemporal C-band radar measurements on wheat fields," *IEEE Trans. Geosci. Remote Sens.*, vol. 41, no. 7, pp. 1551–1560, Jul. 2003.

[90] M. Zribi et al., "Analysis of L-band SAR data for soil moisture estimations over agricultural areas in the tropics," *Remote Sens.*, vol. 11, no. 9, Jan. 2019, Art. no. 1122. [Online]. Available: https://www.mdpi.com/2072-4292/11/9/1122

[91] K. Kellogg et al., "NASA-ISRO synthetic aperture radar (NISAR) mission," in *IEEE Aerosp. Conf.*, Mar. 2020, pp. 1–21.

[92] J. Inglada, A. Vincent, M. Arias, B. Tardy, D. Morin, and I. Rodes, "Operational high resolution land cover map production at the country scale using satellite image time series," *Remote Sens.*, vol. 9, no. 1, Jan. 2017, Art. no. 95. [Online]. Available: https://www.mdpi.com/2072-4292/9/1/95

[93] A. Orynbaikyzy, U. Gessner, B. Mack, and C. Conrad, "Crop type classification using fusion of Sentinel-1 and Sentinel-2 data: Assessing the impact of feature selection, optical data availability, and parcel sizes on the accuracies," *Remote Sens.*, vol. 12, no. 17, Jan. 2020, Art. no. 2779. [Online]. Available: https://www.mdpi.com/2072-4292/12/17/2779

[94] S. Ofori-Ampofo, C. Pelletier, and S. Lang, "Crop type mapping from optical and radar time series using attention-based deep learning," *Remote Sens.*, vol. 13, no. 22, Jan. 2021, Art. no. 4668. [Online]. Available: https://www.mdpi.com/2072-4292/13/22/4668

[95] L. Blickensdörfer, M. Schwieder, D. Pflugmacher, C. Nendel, S. Erasmi, and P. Hostert, "Mapping of crop types and crop sequences with combined time series of Sentinel-1, Sentinel-2 and Landsat 8 data for Germany," *Remote Sens. Environ.*, vol. 269, Feb. 2022, Art. no. 112831. [Online]. Available: https://www.sciencedirect.com/science/article/pii/S0034425721005514

[96] W. W. Verstraeten et al., "Remotely sensed soil moisture integration in an ecosystem carbon flux model. The spatial implication," in *Greenhouse Gas Inventories: Dealing With Uncertainty*, Dordrecht: Netherlands: Springer, 2011, pp. 117–136.

[97] J. Neupane and W. Guo, "Agronomic basis and strategies for precision water management: A review," *Agronomy*, vol. 9, no. 2, Feb. 2019, Art. no. 87. [Online]. Available: https://www.mdpi.com/2073-4395/9/2/87

[98] P. P. Preetha and A. Z. Al-Hamdan, "Developing nitrate-nitrogen transport models using remotely-sensed geospatial data of soil moisture profiles and wet depositions," *J. Environ. Sci. Health, Part A*, vol. 55, no. 5, pp. 615–628, Apr. 2020, doi: 10.1080/10934529.2020.1724503.

Thomas Weiß received the B.Sc. degree in geography and the M.Sc. degree in environmental systems and sustainability (physical geography) from Ludwig-Maximilians-Universität (LMU), Munich, Germany, in 2012 and 2015, respectively.

From 2016, he was a Scientific Staff Member with LMU and contributed to several international projects. In 2023, he joined the newly founded Department of Smart Farming, Fraunhofer Institute for Computer Graphics Research (IGD), Rostock, Germany. His main research interests include data assimilation of microwave and optical remote sensing data to derive and monitor bio- and geophysical parameters for agricultural purposes.

Thomas Jagdhuber (Senior Member, IEEE) received the Diploma degree in physical geography, physics, remote sensing, and geoinformatics from Ludwig-Maximilians-Universität (LMU), Munich, Germany, and the Technical University Munich (TUM), Munich, in 2006, and the Ph.D. degree in hydrology from the Faculty of Science, University of Potsdam, Potsdam, Germany, in 2012.

Since 2007, he has been with the Microwaves and Radar Institute (HR), German Aerospace Center (DLR), Weßling, Germany. From 2014 to 2023, he was a Yearly Visiting Scientist with the Massachusetts Institute of Technology (MIT), Boston, MA, USA, contributing to the preparation and continuation of the Soil Moisture Active Passive (SMAP) and SMAP/Sentinel-1 missions. He is also a Lecturer with the University of Jena, Jena, Germany, and the University of Augsburg, Augsburg, Germany. His main research interests include physics-based multisensor data integration with a focus on active and passive microwave interaction theory and polarimetric techniques for hydrological, agricultural, ecological, and cryospheric parameter modeling and estimation.

Dr. Jagdhuber was the recipient of the DLR Science Award for his research on polarimetric SAR decomposition techniques in 2014, and together with Prof. Entekhabi (MIT), he was the co-recipient of the MIT-MISTI Grant for global water cycle and environmental monitoring using active and passive satellite-based microwave instruments. He also serves as a Reviewer for several international journals and conference boards.

Thomas Ramsauer received the M.Sc. degree in environmental systems and sustainability (physical geography) from Ludwig-Maximilians-Universität (LMU), Munich, Germany, in 2015.

Optical data streams of multi- and hyperspectral sensors and microwave imagery obtained from satellite or drone platforms, as well as in-situ monitoring and field campaigns, are sources for his monitoring efforts. He participated in several international and national funded remote sensing campaigns and projects. His research interests include the monitoring and interpretation through subsequent time series analysis of high-resolution land surface state variables derived from remotely sensed imagery.

Alexander Löw received the M.S. degree in geography and the Ph.D. degree in physical geography from Ludwig-Maximilians-Universität (LMU), Munich, Germany, in 2001 and 2004, respectively.

He was a Full Professor of physical geography and microwave remote sensing with LMU. His research interests included the derivation of quantitative land surface parameters from remote sensing data, the assimilation of remote sensing data into climate and land surface process models, and the evaluation of climate models using observational data.

Philip Marzahn received the Diploma degree from the Christian-Albrechts University of Kiel, Kiel, Germany, where he studied geography, soil science, hydrology, and landscape ecology, in 2007, the Ph.D. degree in physical geography from the Faculty of Geoscience, Ludwig-Maximilians-Universität (LMU), Munich, Germany, in 2013, and the Habilitation degree in physical geography, in 2021, respectively.

Since 2021, he is a Full Professor for geodesy and geoinformatics with the Department of Agricultural and Environmental Sciences. His research interests include the monitoring of bio- and geophysical parameters from multidimensional SAR and optical data,, the uncertainty assessment of such variables, and the retrieval of parameters from remote sensing data across scales using spaceborne, airborne, and drone data in conjunction with wireless sensor networks.

Dr. Marzahn is a frequent Reviewer for international remote sensing journals. He has participated in several international and national funded remote sensing campaigns and projects.